

# Markov-Enforced Discrete Diffusion Model for Digital Semantic Symbol Error Correction

Yoon Huh, *Graduate Student Member, IEEE*, Jeongho Kang, and Wan Choi, *Fellow, IEEE*

**Abstract**—Diffusion models (DMs) have achieved remarkable success across various domains owing to their strong generative and denoising capabilities. Meanwhile, semantic communication based on neural joint source–channel coding (JSCC) has emerged as a promising paradigm for robust and efficient image transmission. However, severe channel noise can still distort the transmitted semantic symbols, resulting in significant performance degradation. Applying DMs to digital semantic symbols, particularly in vector quantization (VQ)-based systems, is fundamentally challenging because the Markov assumption does not hold for the symbol transition dynamics. To address this issue, we introduce SSCDM, a semantic symbol correcting diffusion model whose discrete-time transition dynamics are constructed using solutions from continuous-time Markov chain theory. Furthermore, to promote synergy between DMs and JSCC, our DM structure embeds discrete symbols into a latent feature space using a learned VQ codebook, and a self-organizing map-based loss is incorporated during codebook learning to enhance the geometric vicinity between neighboring digital symbols, thereby promoting topology-preserving semantic representations. Experimental results show that the proposed method significantly improves image reconstruction quality and outperforms previous symbol-level denoising techniques under low signal-to-noise ratio scenarios and different datasets.

**Index Terms**—continuous-time Markov chain, discrete diffusion model, vector quantization, digital semantic communication, self-organizing map.

## I. INTRODUCTION

Diffusion models (DMs) [1]–[5] have been widely adopted across diverse fields such as image and video synthesis, molecular design, and scientific data modeling, opening new avenues for solving complex engineering problems [6]. Originally developed for generative modeling, DMs can be broadly categorized according to the domain of the data they operate on. Continuous DMs [1], [2] operate on continuous-valued data, where the forward process progressively corrupts continuous data by injecting noise, and a reverse denoising process is learned to iteratively recover clean representations from noisy observations. In contrast, discrete DMs [3]–[5] are designed for data represented by discrete states. In this case, the forward process perturbs the data through state transitions governed by transition probability matrices across successive steps, and the reverse process reconstructs the original data by reversing these state perturbations. Importantly, both continuous and discrete DMs are fundamentally built upon a Markovian

forward process, which ensures theoretical tractability and enables computationally efficient training and inference.

Although initially introduced for data generation tasks, DMs provide a unified framework for progressively modeling and reversing data corruption in both continuous and discrete domains. This property naturally aligns with wireless communication systems, where channel impairments can be interpreted as the corruption applied to transmitted signals or symbols. In principle, DMs can therefore be utilized either for continuous signal denoising at the receiver or for discrete symbol correction after detection. However, despite this clear conceptual compatibility, diffusion-based approaches remain largely unexplored in conventional wireless communication systems for the reliable transmission of random bitstreams.

Meanwhile, as sixth-generation (6G) networks shift toward task-oriented paradigms [7] that demand higher spectral efficiency, semantic communication [8] has emerged as a promising solution. Unlike conventional systems that aim to faithfully transmit raw data, semantic communication focuses on delivering task-relevant information, thereby reducing redundancy. A key enabler of this paradigm is joint source-channel coding (JSCC) [9]–[11], which integrates source and channel coding into a unified neural network trained end-to-end for robust task performance. While early semantic communication schemes often adopt fully analog or continuous latent representations, practical deployments increasingly favor digital semantic communication for better compatibility with existing infrastructures. In this work, we consider a vector quantization (VQ)-based digital semantic communication system for image transmission [12], [13], where semantic features from a JSCC encoder are quantized via a learned VQ codebook and transmitted as digital symbols. Nevertheless, despite its advantages, JSCC-based semantic communication remains vulnerable in low signal-to-noise ratio (SNR) regimes, where severe channel noise distorts semantic symbols and significantly degrades task performance.

Recently, DMs have been introduced into digital semantic communication to improve task performance under adverse wireless conditions, particularly in low-SNR regimes where semantic distortion is severe [14]–[16]. Existing studies can be divided into two distinct directions: symbol error correction using discrete DMs and symbol denoising using continuous DMs. For symbol error correction, the channel denoising discrete diffusion model (CD3M) proposed in [14], following the discrete DM framework in [3], estimates per-step transition matrices by identifying the best-fitting multiplier between two consecutive symbol detection matrices. While this approach leverages the true observed detection probabilities during the symbol error correction process, it does not explicitly account

This work was supported by Samsung Electronics Co., Ltd (IO251211-14376-01).

Y. Huh, J. Kang and W. Choi are with the Department of Electrical and Computer Engineering, Seoul National University (SNU), and the Institute of New Media and Communications, SNU, Seoul 08826, Korea. (e-mail: {mnihy621, ttomas11, wanchoi}@snu.ac.kr)

(Corresponding Authors: Wan Choi)

for the fact that *the symbol-wise transition dynamics induced by digital communication channels violate the Markov property in the discrete domain*, which constitutes a key finding of this work. Since the outstanding performance of DMs comes from the Markov property, the violation severely limits the attainable performance. Notably, this non-Markovian behavior is an inherent characteristic of digital communication systems and is not specific to semantic communication settings.

Another line of work on symbol error correction is the discrete channel denoising diffusion model (DCDDM) proposed in [15]. It adopts a discrete DM framework [3] and constructs per-step transition matrices heuristically. Specifically, each transition matrix assigns a self-transition probability corresponding to error-free transmission, while the remaining probability mass is distributed across other symbols in proportion to their pairwise symbol error probabilities. Although this design offers a simple and computationally efficient approximation, the resulting transition matrices do not accurately capture the true stochastic behavior of digital communication channels. In particular, the off-diagonal entries do not correspond to true symbol detection error probabilities, and the independently constructed per-step transition matrices fail to *jointly form a coherent Markov chain*, due to violation of the Chapman–Kolmogorov equation.

Consequently, both DCDDM and CD3M rely on transition matrices that do not satisfy the Markov property assumed in the discrete DM framework [3], creating a fundamental mismatch between the modeled diffusion dynamics and the true channel-induced symbol transitions. The strong empirical performance and computational efficiency of DMs fundamentally arise from the Markovian structure of the forward process, which enables tractable training and inference. Retaining these advantages therefore requires strict adherence to this core theoretical premise. When the adopted transition matrices violate this rigorous foundational assumption and diverge from the actual channel dynamics, the resulting structural inconsistency severely constrains the attainable performance. This intrinsic non-Markovian nature of symbol transitions therefore poses a fundamental challenge to applying Markov-based discrete DMs in digital semantic communication, which serves as the central motivation for the proposed approach.

In contrast, continuous DM-based symbol denoising is exemplified by the score-based channel denoising model (SCDM) proposed in [16], built on a continuous DM framework [2]. It directly denoises noisy digital symbols, such as QAM symbols corrupted by Gaussian noise, prior to receiver-side symbol detection. However, SCDM, like the discrete DM-based approaches, operates solely on symbol representations, e.g., coordinates or indices, without *explicitly accounting for the semantic relevance among encoded features*. Consequently, the diffusion module primarily serves as a noise suppressor rather than a semantics-aware component. This inherently constrains performance and hinders effective joint design with semantic communication, leaving substantial untapped potential for improvement. These limitations motivate the development of semantics-informed diffusion architectures and training strategies *explicitly designed in coordination with the JSCC encoder–decoder and the learned VQ codebook*,

enabling more effective learning, improved task performance, and tighter integration with digital semantic communication.

To address the above challenges, we propose a novel semantic symbol correcting diffusion model (SSCDM) tailored for VQ-based digital semantic communication. Within a discrete DM framework [3], the core design objective of SSCDM is to ensure Markov consistency across diffusion steps while preserving the channel-induced symbol transition probabilities. To this end, we leverage the solution structure of continuous-time Markov chain (CTMC) theory [4] as a theoretical foundation for constructing valid state transition dynamics that inherently satisfy the Markov property. Specifically, we enforce the CTMC solution structure across all discrete-time transition matrices and jointly optimize them by minimizing the discrepancy with the true symbol transition matrices. Consequently, the resulting diffusion dynamics constitute a valid Markov process that more accurately reflects realistic digital symbol corruption, enabling a more reliable reverse denoising process and significantly improving semantic reconstruction fidelity.

Furthermore, unlike prior works, SSCDM goes beyond being a simple plug-in symbol error corrector in semantic communication systems. It is explicitly designed to synergize with the JSCC framework by accounting for the latent feature space structured by the learned VQ codebook in two key aspects: latent-aware DM input embedding and a Gray-mapped codebook formulation. Specifically, SSCDM does not directly feed symbol index vectors into the DM. Rather, it first maps each index to its corresponding codeword via the learned VQ codebook, thereby forming a codeword tensor representation. The DM then operates on this semantic feature tensor, enabling it to interpret the detected symbols in a manner consistent with how the JSCC model represents semantic information. By this embedding process, SSCDM enables semantically informed and coherent diffusion-based symbol correction while preserving the discrete nature of the transmitted symbols.

As another point of synergy, we regulate the VQ codebook training to preserve the topology of constellation symbols. A VQ codebook trained without explicit inter-codeword regularization does not necessarily preserve geometric continuity or semantic consistency among neighboring symbols, unlike Gray mapping in conventional digital modulation. As a result, imperfect symbol error correction, where a misdetected symbol is moved closer to the true constellation point but does not exactly reach it, does not reliably lead to improved reconstruction performance. Although [17] proposed a heuristic post-training approach that greedily reorders learned codewords based on Euclidean distance, such a method lacks theoretical grounding and can result in suboptimal or unstable performance. To mitigate this issue, we incorporate a self-organizing map (SOM)–based loss [18], [19], which encourages neighboring constellation symbols to be associated with semantically similar codewords. This topology-preserving constraint enforces geometric and semantic consistency within the codebook, thereby further strengthening the coupling between the VQ codebook, the diffusion-based symbol correction, and the JSCC decoder. As a result, SSCDM achieves more stable symbol correction and yields substantial performance gains, particularly in low-SNR regimes.

**Contributions.** This paper contributes as follows:

- **Transition dynamics analysis:** We analyze the inherent challenge of modeling symbol-wise transition dynamics in VQ-based digital semantic communication, highlighting the violation of the Markov property in the discrete symbol domain under digital communication channels.
- **Markov-enforced digital symbol correction method:** We propose SSCDM, a novel symbol correction framework that enforces valid Markov transition dynamics for discrete symbols by constructing discrete-time diffusion transitions from the CTMC solutions, enabling principled and robust symbol correction under channel noise.
- **Neural architecture leveraging learned VQ codebook:** We design a neural JSCC architecture that utilizes a learned VQ codebook to embed discrete symbols into a continuous latent space, allowing effective diffusion-based correction with improved semantic consistency.
- **Topology-preserving VQ regularization:** To enhance the geometric consistency of the learned VQ codebook and ensure topology-preserving symbol mapping, we integrate a SOM-based regularization loss into the training, which effectively improves semantic continuity and correction robustness.
- **Comprehensive experiments:** We conduct extensive experiments across various channel conditions and datasets, demonstrating the superiority of our SSCDM in terms of semantic fidelity and robustness over existing approaches.

**Notations.** Vectors and matrices are expressed in lower case and upper case bold, respectively.  $\|\cdot\|_p$  denotes the  $l_p$  norm of a vector.  $\mathbb{R}$  represents the real number set.  $[a:b]$  is an integer set of  $\{a, a+1, \dots, b\}$ .  $[\cdot]^T$  denotes the transpose of a matrix or vector.  $[\mathbf{A}]_{i,j}$  and  $[\mathbf{a}]_i$  denote the  $(i, j)$ -th entry of  $\mathbf{A}$  and the  $i$ -th entry of  $\mathbf{a}$ , respectively.  $[\mathbf{A}]_{i,:}$  and  $[\mathbf{A}]_{:,j}$  denote the  $i$ -th row and the  $j$ -th column of  $\mathbf{A}$ , respectively.  $\mathcal{CN}(\boldsymbol{\mu}, \boldsymbol{\Sigma})$  is a complex Gaussian distribution with mean vector  $\boldsymbol{\mu}$  and covariance matrix  $\boldsymbol{\Sigma}$ .  $\mathbf{I}_m$  and  $\mathbf{1}_m$  represent the  $m \times m$  identity matrix and the  $m$ -dimensional all-ones vector, respectively.  $\mathbb{E}[\cdot]$  denotes the expected value of a given random variable.

## II. PRELIMINARIES

### A. Discrete Diffusion Model

Analogous to the continuous DM [1], which removes Gaussian noise through a reverse process learned from a predefined forward noise process, the discrete DM [3] is designed to reverse the stochastic transitions applied to perturbed discrete-valued data, as illustrated in Fig. 1(c). The forward process is Markovian and defined over a finite set of discrete states. In this subsection, we adopt a discrete-time formulation in which transitions occur step-by-step over fixed time steps.

For  $M$ -categorical scalar random variables<sup>1</sup>  $u_{t_k}, u_{t_{k-1}} \in [1:M]$ , the forward state transition matrix  $\mathbf{Q}_{t_k|t_{k-1}} \in \mathbb{R}^{M \times M}$  from time point  $t_{k-1}$  to  $t_k$  is defined as  $[\mathbf{Q}_{t_k|t_{k-1}}]_{i,j} = q_{t_k|t_{k-1}}(u_{t_k} = j | u_{t_{k-1}} = i)$ , where  $0 \leq t_{k-1} < t_k \leq 1$  for  $k \in [1:T]$  and  $T$  is a total number of time steps. Here,

<sup>1</sup>For clarity, we describe the formulation in the one-dimensional case. Extensions to the multi-dimensional setting can be found in existing works on discrete DMs, such as [3], [4].

$u_{t_0}$  denotes the original data sampled from  $q_{t_0}(u) = p_{\text{data}}(u)$ , i.e., training dataset, and  $u_{t_T}$  represents the fully perturbed data following  $q_{t_T}(u)$ , which is a known stationary distribution approximated by  $p_{\text{ref}}(u)$  for ease of sampling.

Using the one-hot encoding of  $u$ , i.e., a row vector  $\mathbf{w} \in \mathbb{R}^{1 \times M}$ , the transition probability can be written as  $q_{t_k|t_{k-1}}(u_{t_k}|u_{t_{k-1}}) = \text{Cat}(\mathbf{w}_{t_k}; \mathbf{p} = \mathbf{w}_{t_{k-1}} \mathbf{Q}_{t_k|t_{k-1}})$ , where  $\text{Cat}(\mathbf{w}; \mathbf{p})$  denotes the categorical distribution over  $\mathbf{w}$  with class probabilities given by the row vector  $\mathbf{p} \in \mathbb{R}^{1 \times M}$ . This leads to the  $k$ -step marginal:  $q_{t_k|t_0}(u_{t_k}|u_{t_0}) = \text{Cat}(\mathbf{w}_{t_k}; \mathbf{p} = \mathbf{w}_{t_0} \mathbf{Q}_{t_k|t_0})$ , where  $\mathbf{Q}_{t_k|t_0} = \prod_{i=1}^k \mathbf{Q}_{t_i|t_{i-1}} \in \mathbb{R}^{M \times M}$  is the accumulated transition matrix up to time  $t_k$ . Then, the full forward Markov process is described by  $q_{t_0:t_T}(u_{t_0:t_T}) = p_{\text{data}}(u_{t_0}) \prod_{k=1}^T q_{t_k|t_{k-1}}(u_{t_k}|u_{t_{k-1}})$ .

On the other hand, the reverse process can be expressed as  $q_{t_0:t_T}(u_{t_0:t_T}) = q_{t_T}(u_{t_T}) \prod_{k=1}^T q_{t_{k-1}|t_k}(u_{t_{k-1}}|u_{t_k})$ , where  $q_{t_{k-1}|t_k} = q_{t_k|t_{k-1}} \frac{q_{t_{k-1}}}{q_{t_k}}$ . However, in practice, this reverse kernel  $q_{t_{k-1}|t_k}$  is generally intractable, since evaluating the marginal distribution  $q_{t_k}$  requires integrating over the true data distribution  $p_{\text{data}}$ , which is unknown and not available in closed form, i.e.,  $q_{t_k}(u_{t_k}) = \int q_{t_k|t_0}(u_{t_k}|u_{t_0}) p_{\text{data}}(u_{t_0}) du_{t_0}$ . Thus, it is approximated by training an NN-based reverse kernel  $p_{t_{k-1}|t_k}^\theta$ , which is parameterized by  $\theta$ . A common approach is to define the reverse kernel via the conditional distribution  $q_{t_{k-1}|t_k, t_0}$  as follows:

$$\begin{aligned} p_{t_{k-1}|t_k}^\theta(u_{t_{k-1}}|u_{t_k}) \\ = \sum_{u_{t_0}=1}^M q_{t_{k-1}|t_k, t_0}(u_{t_{k-1}}|u_{t_k}, u_{t_0}) p_{t_0|t_k}^\theta(u_{t_0}|u_{t_k}), \end{aligned} \quad (1)$$

where  $q_{t_{k-1}|t_k, t_0} = q_{t_k|t_{k-1}} \frac{q_{t_{k-1}|t_0}}{q_{t_k|t_0}}$ . The full reverse process is then approximated as  $p_{t_0:t_T}^\theta(u_{t_0:t_T}) = p_{\text{ref}}(u_{t_T}) \prod_{k=1}^T p_{t_{k-1}|t_k}^\theta(u_{t_{k-1}}|u_{t_k})$ .

The training loss function  $\mathcal{L}_{\text{DT}}$  [3], primarily based on the formulation in [1], is defined as

$$\begin{aligned} \mathcal{L}_{\text{DT}} = \mathbb{E}_{p_{\text{data}}} \left[ -\mathbb{E}_{q_{t_1|t_0}} \log p_{t_0|t_1}^\theta(u_{t_0}|u_{t_1}) + \sum_{k=2}^T \mathbb{E}_{q_{t_k|t_0}} \right. \\ \left. [\text{KL}(q_{t_{k-1}|t_k, t_0}(u_{t_{k-1}}|u_{t_k}, u_{t_0}) || p_{t_{k-1}|t_k}^\theta(u_{t_{k-1}}|u_{t_k}))] \right], \end{aligned} \quad (2)$$

which serves as an upper bound on the negative log-likelihood  $\mathbb{E}_{p_{\text{data}}}[-\log q_{t_0}(u_{t_0})]$ . Here, the first term evaluates how accurately the model reconstructs the original data from the last single reverse step. Meanwhile, the KL term guides the model to approximate the true posterior  $q_{t_{k-1}|t_k, t_0}$  across all steps, providing a ground-truth trajectory for the reverse transition since the true reverse kernel  $q_{t_{k-1}|t_k}$  is intractable without conditioning on the original data  $u_{t_0}$ . To further enhance performance, a direct generative loss term is introduced:

$$\mathcal{L}_{\text{G}} = \mathbb{E}_{p_{\text{data}}} \left[ \mathbb{E}_{q_{t_k|t_0}} [-\log p_{t_0|t_k}^\theta(u_{t_0}|u_{t_k})] \right], \quad (3)$$

which encourages the model to directly estimate the original data from noisy states sampled at arbitrary time steps, complementing the KL term in (2) by explicitly considering the learned reverse kernel in (1). The overall objective is given by

$$\mathcal{L}_\lambda = \mathcal{L}_{\text{DT}} + \lambda \mathcal{L}_{\text{G}}, \quad (4)$$

where  $\lambda$  is a hyperparameter that balances the two terms.

### B. Continuous-Time Markov Chain

Under the concept of CTMC [4], [5], state transitions can occur at any time  $t \in [0, 1]$ , unlike the discrete-time Markov process in the previous subsection where transitions happen only at predefined time points  $\{t_k\}_{k=0}^T$ . Given an initial distribution  $q_0 = p_{\text{data}}$ , the CTMC forward process is characterized by a time-dependent rate matrix  $\vec{\mathbf{R}}_t \in \mathbb{R}^{M \times M}$ , which defines the instantaneous transition rates between states:  $[\vec{\mathbf{R}}_t]_{\tilde{u}, u} = \vec{r}_t(u|\tilde{u}) = \lim_{\Delta t \rightarrow 0} \frac{q_{t|t-\Delta t}(u|\tilde{u}) - \delta_{u,\tilde{u}}}{\Delta t}$ , where  $\delta_{u,\tilde{u}}$  is the Kronecker delta, equal to 1 if  $u = \tilde{u}$  and 0 otherwise. Intuitively, at rate  $[\vec{\mathbf{R}}_t]_{\tilde{u}, u}$ , the categorical probability flows from state  $\tilde{u}$  to  $u$ , or equivalently, the state  $\tilde{u}$  is instantaneously transitions to  $u$ . Accordingly,  $\delta_{u,\tilde{u}}$  ensures that the probability of remaining in the same state is properly accounted for, so that the sum of each row of the rate matrix is zero. Equivalently, the infinitesimal transition probability can be expressed as  $q_{t|t-\Delta t}(u|\tilde{u}) = \delta_{u,\tilde{u}} + [\vec{\mathbf{R}}_t]_{\tilde{u}, u} \Delta t + o(\Delta t)$ . Thus, the rate matrix satisfies the following properties.

**Proposition 1** (Rate matrix properties). *For the CTMC forward rate matrix, it holds that*

- 1)  $\vec{r}_t(u|\tilde{u}) \geq 0$  for  $u \neq \tilde{u}$ ,
- 2)  $\vec{r}_t(u|u) \leq 0$ ,
- 3)  $\vec{r}_t(u|u) = -\sum_{u \neq \tilde{u}} \vec{r}_t(u|\tilde{u})$ .

Meanwhile, for  $t > s$ , the transition matrix  $\mathbf{Q}_{t|s}$  and the rate matrix  $\vec{\mathbf{R}}_t$  are related by the Kolmogorov forward equation:  $\partial_t q_{t|s}(u|\tilde{u}) = \sum_{u'} q_{t|s}(u'|\tilde{u}) \vec{r}_t(u|u')$ , which can be written in matrix form as  $\partial_t \mathbf{Q}_{t|s} = \mathbf{Q}_{t|s} \vec{\mathbf{R}}_t$ . If the rate matrices  $\vec{\mathbf{R}}_t$  and  $\vec{\mathbf{R}}_s$  commute for all  $t$  and  $s$ , the solution can be expressed via eigen-decomposition and the matrix exponential  $\exp(\cdot)$ :

$$\mathbf{Q}_{t|0} = \mathbf{V} \mathbf{D}(t) \mathbf{V}^{-1}, \quad (5)$$

$$\vec{\mathbf{R}}_t = \mathbf{V} \boldsymbol{\Sigma}(t) \mathbf{V}^{-1}, \quad (6)$$

where  $\mathbf{D}(t) = \exp(\int_0^t \boldsymbol{\Sigma}(t') dt') \in \mathbb{R}^{M \times M}$  and  $\boldsymbol{\Sigma}(t) \in \mathbb{R}^{M \times M}$  are diagonal matrices, and  $\mathbf{V} \in \mathbb{R}^{M \times M}$  is the eigenvector matrix. Consequently, the sub-transition matrix from time  $s$  to  $t$  can be expressed as

$$\mathbf{Q}_{t|s} = \mathbf{V} \exp\left(\int_s^t \boldsymbol{\Sigma}(t') dt'\right) \mathbf{V}^{-1}. \quad (7)$$

### III. SYSTEM MODEL

Consider a point-to-point digital semantic communication system for image transmission, which especially incorporates a discrete DM at the receiver to enhance robustness against detection errors on digital symbols caused by channel noise. The system employs an NN-based JSCC encoder and decoder, a VQ codebook, and a discrete DM. The overall communication procedure is as follows and summarized by Fig. 1.

At the transmitter side, the source image  $\mathbf{X} \in \mathbb{R}^{C \times H \times W}$ , where  $C$ ,  $H$ , and  $W$  represent the number of tensor channels, height, and width of the image, respectively, is passed through an encoder  $f_{\psi_{\text{Tx}}}$  parameterized by  $\psi_{\text{Tx}}$ . This encoder converts the image into a collection of feature vectors  $\mathbf{Y} = [\mathbf{y}_1, \mathbf{y}_2, \dots, \mathbf{y}_N]^T \in \mathbb{R}^{N \times d}$ , where  $N$  is the number of feature vectors and  $d$  denotes their dimensionality. Formally, this encoding step is given by  $\mathbf{Y} = f_{\psi_{\text{Tx}}}(\mathbf{X})$ .

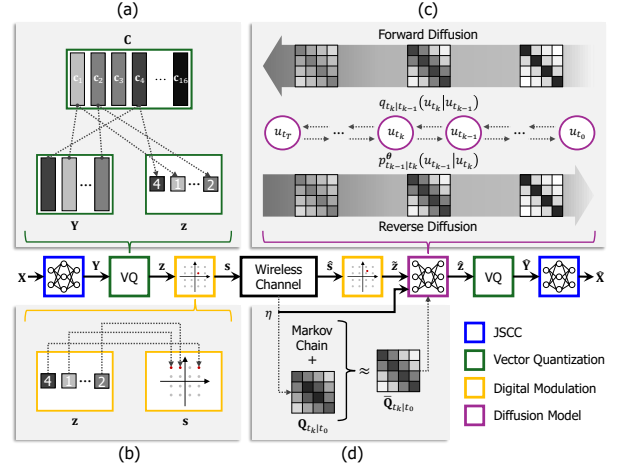


Fig. 1. An illustration of (a) vector quantization ( $M = 16$ ), (b) constellation symbol mapping ( $M = 16$ ), (c) forward and reverse diffusion processes ( $M = 4$ ), and (d) the design philosophy of the proposed discrete diffusion model ( $M = 4$ ). Note that the value of  $M$  differs in (a)–(d) for visualization purposes only, while it should remain consistent throughout the actual system.

Next, these feature vectors  $\mathbf{Y}$  are quantized to produce a codeword index vector  $\mathbf{z} = [z_1, z_2, \dots, z_N]^T \in [1:M]^N$ , with  $M$  being the size of the codebook or digital modulation order. As shown in Fig. 1(a), the quantization uses a learned codebook  $\mathbf{C} = [\mathbf{c}_1, \mathbf{c}_2, \dots, \mathbf{c}_M]^T \in \mathbb{R}^{M \times d}$ , selecting the nearest codeword to each feature vector  $\{\mathbf{y}_i\}_{i=1}^N$  based on Euclidean distance, i.e.,  $z_i = \arg \min_j \|\mathbf{y}_i - \mathbf{c}_j\|_2^2$  for each  $i \in [1:N]$ . Each codeword  $\mathbf{c}_j$  corresponds to a symbol  $\mathbf{s}_j$  in the constellation set  $\mathbb{S} = \{\mathbf{s}_1, \mathbf{s}_2, \dots, \mathbf{s}_M\} \in \mathbb{R}^{2 \times M}$ , with the symbol power normalized such that  $\mathbb{E}[\|\mathbf{s}_i\|_2^2] = P$ . As depicted in Fig. 1(b), the index vector  $\mathbf{z}$  is then modulated into a transmitted symbol sequence  $\mathbf{s} = [\mathbf{s}_{z_1}, \mathbf{s}_{z_2}, \dots, \mathbf{s}_{z_N}] \in \mathbb{S}^N$ , which is sent over an additive white Gaussian noise (AWGN) channel. To summarize, the data transformation at the transmitter follows the path:  $\mathbf{X} \xrightarrow{f_{\psi_{\text{Tx}}}} \mathbf{Y} \xrightarrow{\mathbf{C}} \mathbf{z} \xrightarrow{\mathbb{S}} \mathbf{s}$ .

At the receiver side, the transmitted symbol sequence  $\mathbf{s}$  is perturbed by AWGN, i.e.,  $\mathbf{n} \sim \mathcal{CN}(\mathbf{0}_N, \sigma^2 \mathbf{I}_N)$ , yielding the received signal as  $\hat{\mathbf{s}} = \mathbf{s} + \mathbf{n}$ . Based on this noisy observation, a detection process estimates the transmitted symbols, producing  $\bar{\mathbf{s}} = [\mathbf{s}_{\bar{z}_1}, \mathbf{s}_{\bar{z}_2}, \dots, \mathbf{s}_{\bar{z}_N}] \in \mathbb{S}^N$ , where  $\bar{z}_i \in [1:M]$  denotes the detected index for the  $i$ -th symbol. The SNR for this channel is defined as  $\eta = \frac{P}{\sigma^2}$ , where  $P$  is the average symbol power.

To compensate for the symbol detection errors caused by noise, a discrete DM,  $\text{DM}_\theta$  parameterized by  $\theta$ , is employed to refine the perturbed index sequence  $\tilde{\mathbf{z}} = [\tilde{z}_1, \tilde{z}_2, \dots, \tilde{z}_N]^T \in [1:M]^N$ . Each index  $\tilde{z}_i$  corresponds to the  $M$ -categorical random variable  $u_{t_k}$  in Fig. 1(c), representing a noise-perturbed state. The model progressively corrects the corrupted state and produces a restored index vector  $\hat{\mathbf{z}} = [\hat{z}_1, \hat{z}_2, \dots, \hat{z}_N]^T \in [1:M]^N$ . This reverse diffusion process is expressed as  $\hat{\mathbf{z}} = \text{DM}_\theta(\tilde{\mathbf{z}}, \eta, \mathbf{C})$ , where the SNR value  $\eta$  determines the number of denoising steps, i.e., the starting time point  $t_k$ , according to the severity of index perturbation. Notably, the proposed diffusion model performs semantic-aware processing by leveraging the learned codebook  $\mathbf{C}$ , which is detailed in Section IV-C. Consequently,  $\text{DM}_\theta$  interprets the detected symbol indices  $\tilde{\mathbf{z}}$  in a manner consistent with the semantic feature representation of the JSCC framework. Each restored index  $\hat{z}_i$  corresponds to

$u_{t_0}$  in Fig. 1(c), denoting the clean target state in the reverse diffusion trajectory.

From the restored indices  $\hat{\mathbf{z}}$ , the receiver reconstructs the quantized feature vectors  $\hat{\mathbf{Y}} = [\mathbf{c}_{\hat{\mathbf{z}}_1}, \mathbf{c}_{\hat{\mathbf{z}}_2}, \dots, \mathbf{c}_{\hat{\mathbf{z}}_N}]^T \in \mathbb{R}^{N \times d}$  by referencing the same codebook  $\mathbf{C}$  used at the transmitter. Finally, a decoder  $g_{\psi_{\text{Rx}}}$ , parameterized by  $\psi_{\text{Rx}}$ , transforms the recovered features into the reconstructed image  $\hat{\mathbf{X}} \in \mathbb{R}^{C \times H \times W}$ . This decoding step can be expressed as  $\hat{\mathbf{X}} = g_{\psi_{\text{Rx}}}(\hat{\mathbf{Y}})$ . The data flow at the receiver can be outlined as follows:  $\hat{\mathbf{s}} \xrightarrow{\text{Detection}} \bar{\mathbf{s}} \xrightarrow{\mathbb{S}} \hat{\mathbf{z}} \xrightarrow{\text{DM}_{\theta}} \hat{\mathbf{z}} \xrightarrow{\mathbf{C}} \hat{\mathbf{Y}} \xrightarrow{g_{\psi_{\text{Rx}}}} \hat{\mathbf{X}}$ .

#### IV. SEMANTIC SYMBOL ERROR CORRECTING DISCRETE DIFFUSION MODEL

##### A. Discussions on Transition Matrix Design

In a discrete diffusion process for VQ-based semantic communication, the forward transition matrices  $\{\mathbf{Q}_{t_k|t_{k-1}}\}_{k=1}^T$  should reflect the true state transition probabilities of the constellation symbols in  $\mathbb{S}$  when experiencing Gaussian noise. Based on this principle, the following conditions must hold.

**Proposition 2** (Transition matrix condition). *Let  $\sigma_{t_k}^2$  denote the Gaussian noise variance added from time point  $t_{k-1}$  to  $t_k$  for  $k \in [1:T]$  with  $\sigma_{t_0}^2 = 0$ . Given this predefined noise variance sequence  $\{\sigma_{t_k}^2\}_{k=1}^T$ , the transition matrices for symbols corrupted by Gaussian noise must satisfy*

$$[\mathbf{Q}_{t_k|t_0}]_{i,j} = \iint_{\mathbb{A}_j} \frac{1}{2\pi\sigma_{t_k}^2} e^{-\frac{\|\mathbf{x}-\mathbf{s}_i\|_2^2}{\sigma_{t_k}^2}} d\mathbf{x},$$

representing the transition probability from a single point  $\mathbf{s}_i$  to a region  $\mathbb{A}_j$ , where  $\mathbb{A}_j$  is the decision region for the  $j$ -th symbol  $\mathbf{s}_j$  and  $\sigma_{t_k}^2$  is a cumulative noise variance of  $\sum_{\ell=1}^k \sigma_{t_\ell}^2$ . For  $k \in [2:T]$ , the following must also hold:

$$[\mathbf{Q}_{t_k|t_{k-1}}]_{i,j} = \iint_{\mathbb{A}_i} \frac{a_{t_{k-1}}(\mathbf{x})}{b_{t_{k-1}}(i)} \iint_{\mathbb{A}_j} \frac{1}{2\pi\sigma_{t_k}^2} e^{-\frac{\|\mathbf{x}'-\mathbf{x}\|_2^2}{\sigma_{t_k}^2}} d\mathbf{x}' d\mathbf{x},$$

corresponding to the transition probability from a region  $\mathbb{A}_i$  to a region  $\mathbb{A}_j$ , where  $a_{t_k}(\mathbf{x})$  denotes the marginal distribution over the constellation at time  $t_k$ , expressed as  $a_{t_k}(\mathbf{x}) = \sum_{u=1}^M \frac{q_{t_0}(u)}{2\pi\sigma_{t_k}^2} e^{-\frac{\|\mathbf{x}-\mathbf{s}_u\|_2^2}{\sigma_{t_k}^2}}$ , and  $b_{t_k}(i)$  is a normalization factor for  $a_{t_k}(\mathbf{x})$  in a region  $\mathbb{A}_i$ , such as  $b_{t_k}(i) = \iint_{\mathbb{A}_i} a_{t_k}(\mathbf{x}) d\mathbf{x}$ .

However, it turns out that any sequence of transition matrices satisfying the above conditions is inherently non-Markovian, as shown in the following theorem.

**Theorem 1.** *The transition matrices that satisfy the conditions in Proposition 2 do not form a Markov chain.*

*Proof:* See Appendix A. ■

**Remark 1.** *Following Proposition 2 with a uniformly distributed prior  $q_{t_0}$ , the violation of Markov property can also be numerically examined using the Frobenius norm error, i.e.,  $e_{t_{k_2}|t_{k_1}} = \|\mathbf{Q}_{t_{k_2}|t_0} - \mathbf{Q}_{t_{k_1}|t_0} \mathbf{Q}_{t_{k_2}|t_{k_1}}\|_F$  for  $t_0 < t_{k_1} < t_{k_2}$ . While  $\mathbf{Q}_{t_{k_1}|t_0}$  and  $\mathbf{Q}_{t_{k_2}|t_0}$  are obtained analytically,  $\mathbf{Q}_{t_{k_2}|t_{k_1}}$  is estimated via Monte Carlo (MC) simulation with  $10^6$  samples per QAM symbol. For the time pairs  $(t_{k_1}, t_{k_2}) = (t_9, t_{20})$  and  $(t_{40}, t_{65})$  under the experimental setup in Section VI, the errors are 0.2412 and 0.2603, respectively. These values*

*are considerably larger than the fluctuations from the MC estimation, i.e., 0.0008 and 0.0002, computed as the difference between two independent errors such as  $|e_{t_{k_2}|t_{k_1}}^{(1)} - e_{t_{k_2}|t_{k_1}}^{(2)}|$ .*

This result reveals a fundamental limitation. Although the true transition dynamics under Gaussian noise obey probabilistic integration over continuous space, they do not conform to the Markov property required by most diffusion-based discrete generative models [3], [4]. In practice, this discrepancy between the true noise-induced transition dynamics and the Markov structure assumed by existing DMs can lead to mismatches during training or inference, degrading the performance of symbol error correction in digital semantic communication systems.

##### B. Markov-Enforced Transition Matrices

To address the problem revealed from **Theorem 1**, we propose SSCDM which enforces a Markov property on the correct transition matrices  $\{\mathbf{Q}_{t_k|t_0}\}_{k=1}^T$  under the predefined noise variance sequence<sup>2</sup>  $\{\sigma_{t_k}^2\}_{k=1}^T$  from **Proposition 2**, as conceptualized in Fig. 1(d). While the proposed SSCDM operates within the discrete-time diffusion framework, we draw inspiration from the CTMC solution in [4], reviewed in Section II-B, to construct valid Markov transition matrices. Specifically, by leveraging the CTMC solution structure, we formulate a set of Markov-enforced, time-sampled transition matrices  $\{\bar{\mathbf{Q}}_{t_k|t_0}\}_{k=1}^T$  in an eigen-decomposed form  $\{\mathbf{V}\mathbf{D}(t_k)\mathbf{V}^{-1}\}_{k=1}^T$ , which are then used to define the discrete-time diffusion process. The resulting transition matrices are obtained by solving the following optimization problem.

$$(P1) \quad \arg \min_{\mathbf{V}, \{\mathbf{D}(t_k)\}_{k=1}^T} \sum_{k=1}^T \|\mathbf{Q}_{t_k|t_0} - \bar{\mathbf{Q}}_{t_k|t_0}\|_F^2, \quad (8a)$$

$$\text{s.t.} \quad \bar{\mathbf{Q}}_{t_k|t_0} = \mathbf{V}\mathbf{D}(t_k)\mathbf{V}^{-1} \text{ for } k \in [1:T], \quad (8b)$$

$$[\bar{\mathbf{Q}}_{t_k|t_0}]_{i,j} \geq 0 \text{ for } i, j \in [1:M], k \in [1:T], \quad (8c)$$

$$[\mathbf{V}]_{:,1} = \mathbf{1}_M, \quad (8d)$$

$$[\mathbf{D}(t_k)]_{1,1} = 1 \text{ for } k \in [1:T], \quad (8e)$$

$$[\mathbf{D}(t_k)]_{i,i} \geq 0 \text{ for } i \in [2:M], k \in [1:T]. \quad (8f)$$

(8b) ensures that the approximated matrices follow the CTMC solution structure with the eigen-decomposition in (5), while (8c) enforces the non-negativity of the transition matrix. (8d) and (8e) guarantee that each  $\bar{\mathbf{Q}}_{t_k|t_0}$  is a row-stochastic matrix:  $\sum_{i=1}^M [\bar{\mathbf{Q}}_{t_k|t_0}]_{j,i} = [\bar{\mathbf{Q}}_{t_k|t_0}]_{j,:} \mathbf{1}_M = [\bar{\mathbf{Q}}_{t_k|t_0}]_{j,:} [\mathbf{V}]_{:,1} = [\mathbf{V}]_{j,1} [\mathbf{D}(t_k)]_{1,1} = 1$  for all  $j \in [1:M]$ , where the second equality follows from (8d); the third equality follows from (8b); the last equality follows from (8d) and (8e). This implies  $\bar{\mathbf{Q}}_{t_k|t_0} \mathbf{1}_M = 1 \cdot \mathbf{1}_M$ . Since eigenvectors have scaling freedom and the eigenvector corresponding to the unit eigenvalue must be parallel to  $\mathbf{1}_M$ , we set the first eigenvalue–eigenvector pair to  $(1, \mathbf{1}_M)$  without loss of generality. Lastly, (8f) is needed when considering  $\mathbf{D}(t) = \exp(\int_0^t \Sigma(t') dt')$ .

Certainly, although the approximated solution matrices for the discrete DM define a slightly altered symbol detection

<sup>2</sup>We adopt a sigmoid-based scheduling function [20], as its smooth and non-linear noise allocation enables stable reverse diffusion under varying channel SNR conditions. Details are provided in Appendix D.

region, the receiver still performs symbol detection using the optimal region. Moreover, the optimized transition matrices closely approximate the true symbol detection matrices, resulting in superior reconstruction quality by satisfying the Markov property, as demonstrated in Section VI.

**Remark 2.** Although P1 is formulated to derive the time-sampled CTMC solution, we emphasize that the resulting transition matrices are fully compatible with a discrete-time Markov diffusion process. Recalling (5) and (7), for any pair of discrete time indices  $0 \leq k < \ell \leq T$ , we obtain

$$\begin{aligned}\bar{\mathbf{Q}}_{t_\ell|t_k} &= \mathbf{V} \exp\left(\int_{t_k}^{t_\ell} \boldsymbol{\Sigma}(t') dt'\right) \mathbf{V}^{-1} \\ &= \mathbf{V} \exp\left(\int_0^{t_\ell} \boldsymbol{\Sigma}(t') dt' - \int_0^{t_k} \boldsymbol{\Sigma}(t') dt'\right) \mathbf{V}^{-1} \\ &= \mathbf{V} \exp\left(\int_0^{t_k} \boldsymbol{\Sigma}(t') dt'\right)^{-1} \exp\left(\int_0^{t_\ell} \boldsymbol{\Sigma}(t') dt'\right) \mathbf{V}^{-1} \\ &= \mathbf{V} \mathbf{D}(t_k)^{-1} \mathbf{V}^{-1} \cdot \mathbf{V} \mathbf{D}(t_\ell) \mathbf{V}^{-1} \\ &= \bar{\mathbf{Q}}_{t_k|t_0}^{-1} \bar{\mathbf{Q}}_{t_\ell|t_0},\end{aligned}$$

where the first equality follows from (7); the third equality follows from the fact that  $\boldsymbol{\Sigma}(t)$  is diagonal; the fourth equality follows from the definition of  $\mathbf{D}(t)$  together with the identity  $\mathbf{I}_M = \mathbf{V}^{-1} \mathbf{V}$ ; the last equality follows from (5). As a consequence, the Chapman-Kolmogorov equation holds, i.e.,  $\bar{\mathbf{Q}}_{t_\ell|t_0} = \bar{\mathbf{Q}}_{t_k|t_0} \bar{\mathbf{Q}}_{t_\ell|t_k}$ . Therefore, the sequence  $\{\bar{\mathbf{Q}}_{t_k|t_0}\}_{k=0}^T$  defines a consistent discrete-time Markov process, despite being constructed using a CTMC solution.

Unfortunately, P1 is nonconvex and involves a large number of time steps  $T$ , which makes an optimization procedure computationally difficult. In addition, jointly estimating all transition matrices at once may lead to suboptimal approximations due to accumulated fitting errors. To address these challenges, we sample a subsequence  $\{t_{k_\ell}\}_{\ell=1}^{T'}$  including  $T'$  time steps with  $T' < T$ , where  $k_\ell \in [1:T]$  and  $k_{T'} = T$ , and solve the following reduced problem as an initial step.

$$\begin{aligned}\text{(P2)} \quad & \arg \min_{\mathbf{V}, \{\mathbf{D}(t_{k_\ell})\}_{\ell=1}^{T'}} \sum_{\ell=1}^{T'} \|\mathbf{Q}_{t_{k_\ell}|t_0} - \bar{\mathbf{Q}}_{t_{k_\ell}|t_0}\|_F^2, \\ \text{s.t.} \quad & \bar{\mathbf{Q}}_{t_{k_\ell}|t_0} = \mathbf{V} \mathbf{D}(t_{k_\ell}) \mathbf{V}^{-1} \text{ for } \ell \in [1:T'], \\ & [\bar{\mathbf{Q}}_{t_{k_\ell}|t_0}]_{i,j} \geq 0 \text{ for } i, j \in [1:M], \ell \in [1:T'], \\ & [\mathbf{V}]_{:,1} = \mathbf{1}_M, \\ & [\mathbf{D}(t_{k_\ell})]_{1,1} = 1 \text{ for } \ell \in [1:T'], \\ & [\mathbf{D}(t_{k_\ell})]_{i,i} \geq 0 \text{ for } i \in [2:M], \ell \in [1:T'].\end{aligned}\tag{9}$$

P2 estimates only the coarse-grained transition matrices  $\{\bar{\mathbf{Q}}_{t_{k_\ell}|t_0}\}_{\ell=1}^{T'}$  under  $\{\sigma_{t_{k_\ell}}^2\}_{\ell=1}^{T'}$ , rather than the full set  $\{\bar{\mathbf{Q}}_{t_k|t_0}\}_{k=1}^T$ . To solve this optimization, we adopt a block coordinate descent strategy using the Adam optimizer, where the common eigenvector matrix  $\mathbf{V}$  and the set of diagonal

---

### Algorithm 1 Block coordinate descent algorithm for P2

---

- 1: **Input:** Transition matrices  $\{\mathbf{Q}_{t_{k_\ell}|t_0}\}_{\ell=1}^{T'}$ , weight hyperparameters  $\lambda_1$  and  $\lambda_2$
  - 2: Initialize  $\mathbf{V}$  with  $[\mathbf{V}]_{:,1} = \mathbf{1}_M$  and  $\{\text{diag}(\mathbf{D}(t_{k_\ell}))\}_{\ell=1}^{T'}$  with  $[\mathbf{D}(t_{k_\ell})]_{1,1} = 1$  and  $[\mathbf{D}(t_{k_\ell})]_{i,i} \geq 0$
  - 3: Freeze  $[\mathbf{V}]_{:,1}$  and  $\{\mathbf{D}(t_{k_\ell})\}_{\ell=1}^{T'}$  ▷ row-stochasticity
  - 4: **while** not converged **do**
  - 5: **Step 1: Update  $\mathbf{V}$**
  - 6: Freeze  $\{\mathbf{D}(t_{k_\ell})\}_{\ell=1}^{T'}$
  - 7:  $\{\bar{\mathbf{Q}}_{t_{k_\ell}|t_0}\}_{\ell=1}^{T'} \leftarrow \{\mathbf{V} \mathbf{D}(t_{k_\ell}) \mathbf{V}^{-1}\}_{\ell=1}^{T'}$
  - 8: Compute loss  $\mathcal{L}_{P2}$  referring (10)
  - 9: Update  $\mathbf{V}$  via Adam optimizer
  - 10: **Step 2: Update  $\{\mathbf{D}(t_{k_\ell})\}_{\ell=1}^{T'}$**
  - 11: Freeze  $\mathbf{V}$
  - 12:  $\{\bar{\mathbf{Q}}_{t_{k_\ell}|t_0}\}_{\ell=1}^{T'} \leftarrow \{\mathbf{V} \mathbf{D}(t_{k_\ell}) \mathbf{V}^{-1}\}_{\ell=1}^{T'}$
  - 13: Compute loss  $\mathcal{L}_{P2}$  referring (10)
  - 14: Update  $\{\text{diag}(\mathbf{D}(t_{k_\ell}))\}_{\ell=1}^{T'}$  via Adam optimizer
  - 15:  $\{\mathbf{D}(t_{k_\ell})\}_{\ell=1}^{T'} \leftarrow \{\text{ReLU}(\mathbf{D}(t_{k_\ell}))\}_{\ell=1}^{T'}$  ▷ enforce
  - 4: **end while**
  - 5: **Output:** Optimized  $\mathbf{V}$  and  $\{\mathbf{D}(t_{k_\ell})\}_{\ell=1}^{T'}$
- 

matrices  $\{\mathbf{D}(t_{k_\ell})\}_{\ell=1}^{T'}$  are alternatively updated<sup>3</sup>. Through this alternating minimization, we reduce the approximation error between the original transition matrices and their eigen-decomposed counterparts, while retaining the stochastic properties required for valid transition matrices. The overall optimization procedure is detailed in **Algorithm 1**<sup>4</sup>.

The row-stochasticity of  $\{\bar{\mathbf{Q}}_{t_{k_\ell}|t_0}\}_{\ell=1}^{T'}$  is ensured by fixing  $[\mathbf{V}]_{:,1} = \mathbf{1}_M$  and  $[\mathbf{D}(t_{k_\ell})]_{1,1} = 1$  for  $\ell \in [1:T']$ , as described in line 3 of **Algorithm 1**. Accordingly, they remain unchanged during the optimization process. The objective function for the optimization is defined as  $\mathcal{L}_{P2} = \sum_{\ell=1}^{T'} \mathcal{L}_{t_{k_\ell}}$ , where

$$\begin{aligned}\mathcal{L}_{t_k} &= \|\mathbf{Q}_{t_k|t_0} - \bar{\mathbf{Q}}_{t_k|t_0}\|_F^2 + \lambda_1 \|\text{ReLU}(-\bar{\mathbf{Q}}_{t_k|t_0})\|_F^2 \\ &\quad + \lambda_2 \|\text{ReLU}(-\mathbf{D}(t_k))\|_F^2.\end{aligned}\tag{10}$$

Here,  $\lambda_1$  and  $\lambda_2$  are weight hyperparameters, and  $\text{ReLU}(\mathbf{A})$  denotes the element-wise rectified linear unit (ReLU) function defined as  $\max(0, [\mathbf{A}]_{i,j})$  for all entries of a matrix  $\mathbf{A} \in \mathbb{R}^{M \times M}$ . The first term in (10) represents the primary approximation loss. The second term penalizes negative entries in the transition matrix to enforce non-negativity, which is essential for constructing a valid stochastic matrix. The third term induces the non-negativity of the diagonal matrices. In addition, after each update, we explicitly enforce this non-negativity constraint, as written in line 13 of **Algorithm 1**.

To address the original problem P1, once the coarse-grained transition matrices  $\{\bar{\mathbf{Q}}_{t_{k_\ell}|t_0}\}_{\ell=1}^{T'}$  are obtained by solving P2, the remaining intermediate transition matrices are constructed by applying cubic spline interpolation [21] to the diagonal matrices  $\{\mathbf{D}(t_{k_\ell})\}_{\ell=0}^{T'}$ , as shown in Fig. 2. Here, we define

<sup>3</sup>Due to the structural complexity and non-convexity involving matrix inverses, we employ the Adam optimizer, a stochastic gradient descent-based method, within an automatic-differentiation framework. This practical approach simplifies optimization by avoiding complicated or non-trivial derivation of complex matrix gradients while achieving high approximation fidelity, as confirmed in Section VI-A.

<sup>4</sup>A diagonal matrix  $\mathbf{D}(t_k)$  is defined by its diagonal vector  $\text{diag}(\mathbf{D}(t_k)) \in \mathbb{R}^M$ , where  $\text{diag}(\mathbf{A})$  returns the vector containing the diagonal entries of a matrix  $\mathbf{A} \in \mathbb{R}^{M \times M}$ .

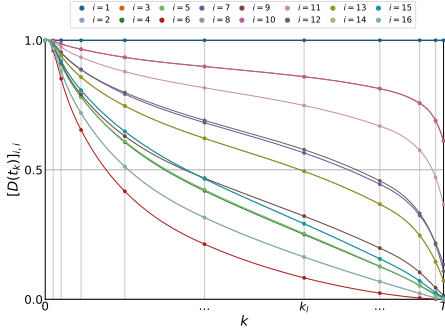


Fig. 2. Diagonal entries of  $\{\mathbf{D}(t_k)\}_{k=0}^T$  obtained via spline interpolation from the optimized subsampled matrices  $\{\mathbf{D}(t_{k_\ell})\}_{\ell=1}^{T'}$  when  $M = 16$ .

$\mathbf{D}(t_0) = \mathbf{I}_M$  based on the identity  $\mathbf{Q}_{t_0|t_0} = \mathbf{I}_M$ . Importantly, the solution of  $\{\mathbf{D}(t_k)\}_{k=1}^T$  from P1 exhibits a consistent property in its diagonal elements, as described below.

**Lemma 1.** Assume that there exist the rate matrices  $\vec{\mathbf{R}}_t$  corresponding to the solution of P1 for  $0 \leq t \leq 1$ . Then, for  $i \in [1:M]$ , a time sequence of each diagonal element, i.e.,  $\{[\mathbf{D}(t_k)]_{i,i}\}_{k=0}^T$ , is non-increasing.

*Proof:* See Appendix B. ■

Following **Lemma 1**, since the coarse-grained sequence  $\{[\mathbf{D}(t_{k_\ell})]_{i,i}\}_{\ell=0}^{T'}$  is non-increasing, the spline interpolation preserves this trend across all intermediate time steps. This guarantees that the final diagonal sequence  $\{[\mathbf{D}(t_k)]_{i,i}\}_{k=0}^T$  also maintains this property, thereby ensuring a physically consistent evolution of the diffusion process over time.

Finally, the approximated transition matrices  $\{\bar{\mathbf{Q}}_{t_k|t_0}\}_{k=1}^T$  are obtained as  $\bar{\mathbf{Q}}_{t_k|t_0} = \mathbf{V}\mathbf{D}(t_k)\mathbf{V}^{-1}$ . Subsequently, the corresponding single-step transition matrix is computed as  $\bar{\mathbf{Q}}_{t_k|t_{k-1}} = \bar{\mathbf{Q}}_{t_{k-1}|t_0}^{-1}\bar{\mathbf{Q}}_{t_k|t_0} = \mathbf{V}\mathbf{D}(t_{k-1})^{-1}\mathbf{D}(t_k)\mathbf{V}^{-1}$  according to (5) and (7). It is worth noting that  $\text{ReLU}(\bar{\mathbf{Q}}_{t_k|t_0})$  and  $\text{ReLU}(\bar{\mathbf{Q}}_{t_k|t_{k-1}})$  must be applied before using them in the discrete DM to ensure non-negativity.

### C. Semantics-Informed Diffusion Model Architecture

For every reverse diffusion step, DMs typically employ the U-Net architecture [22] to obtain the conditional probability  $p_{t_{k-1}|t_k}^\theta(\mathbf{u}_{t_{k-1}}|\mathbf{u}_{t_k}) \in \mathbb{R}^{N \times M}$ , where  $\mathbf{u}_{t_k} \in [1:M]^N$  is the corrupted sample consisting of the state indices  $\{\mathbf{u}_{t_k}[i]\}_{i=1}^N$ . In [3],  $\mathbf{u}_{t_k}$  is directly processed by the U-Net to compute the logits  $\Phi_{t_k} \in \mathbb{R}^{N \times M}$ . A row-wise softmax is then applied as  $p_{t_0|t_k}^\theta(\mathbf{u}_{t_0}|\mathbf{u}_{t_k}) = \text{Softmax}(\Phi_{t_k}) \in \mathbb{R}^{N \times M}$ , which is subsequently used in (1) to compute  $p_{t_{k-1}|t_k}^\theta$ . However,  $\mathbf{u}_{t_k}$  was treated purely as a sequence of categorical indices, despite each index corresponding to a learned codeword in the VQ codebook  $\mathbf{C} \in \mathbb{R}^{M \times d}$ . In this setting, therefore, the U-Net is trained without any explicit knowledge of the semantic structure of the states, limiting its ability to model relationships within the latent feature space.

To enable the DM to better estimate conditional probabilities by exploiting semantic information, we propose incorporating the pretrained VQ codebook  $\mathbf{C}$  into the U-Net input. Specifically, before entering the U-Net,  $\mathbf{u}_{t_k}$  is embedded through the given codebook as  $\mathbf{W}_{t_k}\mathbf{C} \in \mathbb{R}^{N \times d}$ , where  $\mathbf{W}_{t_k} \in \mathbb{R}^{N \times M}$  is a matrix of row-wise one-hot vectors

corresponding to  $\mathbf{u}_{t_k}[i]$  for  $i \in [1:M]$ . This embedding step injects the relational structure among the  $N$  indices from the  $M$  possible states, leveraging the semantic organization already learned in the VQ codebook. As a result, the U-Net can perform probability estimation in a more semantically informed manner, while reflecting the true digital communication channel behavior. Moreover, this embedding mechanism strengthens the integration between the DM and the JSCC structure, which is expected to yield a cooperative effect. Following [3], the final conditional probability  $p_{t_{k-1}|t_k}^\theta$  is obtained by applying the Softmax function to the output logits  $\Phi_{t_k}$  to compute  $p_{t_0|t_k}^\theta$ , and then incorporating it into the reverse kernel modified from (1), given by

$$\begin{aligned} p_{t_{k-1}|t_k}^\theta(u_{t_{k-1}}|u_{t_k}, \mathbf{C}) \\ = \sum_{u_{t_0}=1}^M q_{t_{k-1}|t_k, t_0}(u_{t_{k-1}}|u_{t_k}, u_{t_0}) p_{t_0|t_k}^\theta(u_{t_0}|u_{t_k}, \mathbf{C}). \end{aligned} \quad (11)$$

## V. TRAINING AND INFERENCE ALGORITHMS

### A. Training Method

The proposed discrete DM-aided digital semantic communication is trained through a two-stage procedure that jointly optimizes the JSCC model parameters  $\{\psi_{\text{Tx}}, \psi_{\text{Rx}}\}$ , the VQ codebook  $\mathbf{C}$ , and the DM parameters  $\theta$ . The training utilizes a dataset  $\mathcal{D}$ , approximated transition matrices  $\{\bar{\mathbf{Q}}_{t_k|t_0}\}_{k=1}^T$ , the loss weights  $\{\alpha, \beta, \gamma, \lambda\}$ , and training SNR  $\eta_{\text{train}}$ .

In the first stage, the VQ-based JSCC system without SSCDM is optimized in a mini-batch manner. For each iteration, mini-batch samples are transmitted through an AWGN channel with  $\eta_{\text{train}}$  employing the JSCC encoder  $f_{\psi_{\text{Tx}}}$ , decoder  $g_{\psi_{\text{Rx}}}$ , and learnable codebook  $\mathbf{C}$ . We adopt a reconstruction-based loss function provided in [12]:

$$\begin{aligned} \mathcal{L}_{\text{VQ}} = \mathbb{E}_{\mathbf{X}}[\text{MSE}(\hat{\mathbf{X}}, \mathbf{X}) + \alpha \text{MSE}(\hat{\mathbf{Y}}, \text{sg}(\mathbf{Y})) \\ + \beta \text{MSE}(\mathbf{Y}, \text{sg}(\hat{\mathbf{Y}}))], \end{aligned} \quad (12)$$

where  $\text{MSE}(\mathbf{A}, \mathbf{B})$  represents the mean squared error (MSE) between two inputs  $\mathbf{A}$  and  $\mathbf{B}$ , and  $\text{sg}(\mathbf{A})$  is the stop-gradient operation that prevents the flow of gradients through  $\mathbf{A}$  during backpropagation. Each component of the above loss serves a distinct function:

- The first term ensures that the encoder and decoder reconstruct the input image accurately, accounting for distortions introduced by both the VQ and the channel noise. Since the VQ operation is non-differentiable, a straight-through estimator [23] is employed to enable gradient propagation from  $\mathbf{Y}$  to  $\hat{\mathbf{Y}}$ .
- The second term guides the optimization of the codebook by pulling the quantized output  $\hat{\mathbf{Y}}$  closer to the encoder output  $\mathbf{Y}$ , which has been degraded by channel noise. The stop-gradient on  $\mathbf{Y}$  prevents encoder parameters from being affected during this update.
- The third term acts as a commitment loss, promoting stability of the codebook convergence by encouraging the encoder output  $\mathbf{Y}$  to stay close to its quantized counterpart  $\hat{\mathbf{Y}}$ . The stop-gradient on  $\hat{\mathbf{Y}}$  ensures that only the encoder is updated, leaving the codebook unchanged during this step.

---

**Algorithm 2** Training algorithm
 

---

1: **Input:** Dataset  $\mathcal{D}$ , Markov-enforced transition matrices  $\{\bar{\mathbf{Q}}_{t_k|t_0}\}_{k=1}^T$ , hyperparameters  $\{\alpha, \beta, \gamma, \lambda\}$ , training SNR  $\eta_{\text{train}}$   
 2: Initialize training parameters  $\{\psi_{\text{Tx}}, \psi_{\text{Rx}}, \mathbf{C}, \theta\}$   
**Stage 1: Train JSCC without SSCDM**  
 3: **while** not converged **do**  
 4:   Sample  $\mathbf{X} \in \mathcal{D}$   $\triangleright$  mini-batch data  
 5:   Encode  $\mathbf{X}$  into  $\mathbf{Y}$  using  $f_{\psi_{\text{Tx}}}$   
 6:   Quantize  $\mathbf{Y}$  into  $\mathbf{z}$  using  $\mathbf{C}$  and modulate into  $\mathbf{s}$   
 7:   Receive  $\hat{\mathbf{s}}$  via AWGN channel with  $\eta_{\text{train}}$   
 8:   Demodulate  $\hat{\mathbf{s}}$  into  $\hat{\mathbf{z}}$  and dequantize into  $\hat{\mathbf{Y}}$  using  $\mathbf{C}$   
 9:   Decode  $\hat{\mathbf{Y}}$  into  $\hat{\mathbf{X}}$  using  $g_{\psi_{\text{Rx}}}$   
 10:   Calculate  $\mathcal{L}_{\text{VQ-SOM}}$  as (14)  
 11:   Update  $\{\psi_{\text{Tx}}, \psi_{\text{Rx}}, \mathbf{C}\}$  via Adam optimizer  
 12: **end while**  
**Stage 2: Train SSCDM for symbol error correction**  
 13: Freeze  $\{\psi_{\text{Tx}}, \psi_{\text{Rx}}, \mathbf{C}\}$   
 14: **while** not converged **do**  
 15:   Sample  $\mathbf{X} \in \mathcal{D}$   $\triangleright$  mini-batch data  
 16:   Get  $\mathbf{z}$  from  $\mathbf{X}$  using  $f_{\psi_{\text{Tx}}}$  and  $\mathbf{C}$   
 17:   Define  $\mathbf{u}_{t_0} = \mathbf{z}$   
 18:   Sample  $k \sim \text{Unif}[1:T]$   
 19:   Perturb  $\mathbf{u}_{t_0}$  into  $\mathbf{u}_{t_k}$  using  $\bar{\mathbf{Q}}_{t_k|t_0}$   
 20:   Correct  $\mathbf{u}_{t_k}$  into  $\hat{\mathbf{u}}_{t_0}$  using  $\text{DM}_\theta$   
 21:   Calculate  $\mathcal{L}_\lambda$  as (4)  
 22:   Update  $\theta$  via Adam optimizer  
 23: **end while**  
 24: **Output:** Optimized parameters  $\{\psi_{\text{Tx}}^*, \psi_{\text{Rx}}^*, \mathbf{C}^*, \theta^*\}$

---

After the image reconstruction,  $\mathcal{L}_{\text{VQ}}$  is then computed, and  $\{\psi_{\text{Tx}}, \psi_{\text{Rx}}, \mathbf{C}\}$  are updated via the Adam optimizer.

In the second stage, with the pretrained VQ-based JSCC parameters  $\{\psi_{\text{Tx}}^*, \psi_{\text{Rx}}^*, \mathbf{C}^*\}$  fixed, the discrete DM parameters  $\theta$  are optimized. For each iteration, mini-batch data are encoded into index vectors using the encoder and VQ codebook, where each index vector  $\mathbf{z}$  serves as the clean data sample  $\mathbf{u}_{t_0}$  for the SSCDM training. After a time point  $t_k$  is selected by sampling  $k$  from a discrete uniform distribution  $\text{Unif}[1:T]$ ,  $\mathbf{u}_{t_0}$  is randomly corrupted into  $\mathbf{u}_{t_k}$  by the transition matrix  $\bar{\mathbf{Q}}_{t_k|t_0}$ , which captures the characteristics of digital communication channel while satisfying the Markov property. The perturbed sample  $\mathbf{u}_{t_k}$  is subsequently refined into  $\hat{\mathbf{u}}_{t_0}$  by  $\text{DM}_\theta$ , which first embeds  $\mathbf{u}_{t_k}$  using  $\mathbf{C}$  to exploit the geometry of the learned semantic latent space. The overall training objective of the SSCDM follows  $\mathcal{L}_\lambda$  in (4), and the parameters  $\theta$  of  $\text{DM}_\theta$  are updated using the Adam optimizer.

### B. SOM-based Codebook Learning

In conventional digital modulation, bit sequences are typically Gray-mapped to minimize the Hamming distance between adjacent symbols. However, a VQ codebook trained only with the reconstruction loss in (12) does not inherently preserve such locality in the Euclidean feature space. That is, the codewords corresponding to two neighboring digital symbols may not be closer to each other than those of more distant symbols, unlike the property ensured by Gray-mapping. As a result, although our SSCDM attempts to pull a misdetected symbol index back toward its original one, the corresponding codewords may still be far apart in the feature space. This discrepancy causes a mismatch between the correction capability and the image reconstruction quality,

---

**Algorithm 3** Receiver inference algorithm
 

---

1: **Input:**  $\text{DM}_\theta, g_{\psi_{\text{Rx}}}, \mathbf{C}$ , SNR  $\eta$ , received index vector  $\tilde{\mathbf{z}}$   
 2: Find the correction starting index  $k^*$  from  $\eta$  as (15)  
 3: Define  $\mathbf{u}_{t_{k^*}} = \tilde{\mathbf{z}}$   
 4: **for**  $k = k^*, k^* - 1, \dots, 2$  **do**  
 5:   Compute  $p_{t_{k-1}|t_k}^\theta(\mathbf{u}_{t_{k-1}}|\mathbf{u}_{t_k}, \mathbf{C})$  using  $\text{DM}_\theta$  as (11)  
 6:   Sample  $\mathbf{u}_{t_{k-1}}$  from  $p_{t_{k-1}|t_k}^\theta$   
 7: **end for**  
 8: Compute  $p_{t_0|t_1}^\theta(\mathbf{u}_{t_0}|\mathbf{u}_{t_1}, \mathbf{C})$  using  $\text{DM}_\theta$   
 9:  $\{[\mathbf{u}_{t_0}]_i\}_{i=1}^N \leftarrow \{\arg \max_j p_{t_0|t_1}^\theta([\mathbf{u}_{t_0}]_i = j|\mathbf{u}_{t_1}, \mathbf{C})\}_{i=1}^N$   
 10:  $\hat{\mathbf{z}} \leftarrow \mathbf{u}_{t_0}$   
 11: Dequantize  $\hat{\mathbf{z}}$  into  $\hat{\mathbf{Y}}$  using  $\mathbf{C}$   
 12: Decode  $\hat{\mathbf{Y}}$  into  $\hat{\mathbf{X}}$  using  $g_{\psi_{\text{Rx}}}$   
 13: **Output:** Reconstructed image  $\hat{\mathbf{X}}$

---

since correcting a symbol index does not necessarily yield a semantically similar codeword to the original one.

To alleviate this issue, we incorporate the concept of SOM [18]. Recall that the second term in (12), i.e.,  $\text{MSE}(\hat{\mathbf{Y}}, \text{sg}(\mathbf{Y}))$ , encourages each received codeword  $\mathbf{c}_{\tilde{z}_i}$  to move closer to its corresponding feature vector  $\mathbf{y}_i$ . The SOM mechanism extends this idea by also attracting the neighboring codewords  $\mathbb{N}(\tilde{z}_i)$  on the constellation map toward  $\mathbf{y}_i$ . Here,  $\mathbb{N}(\tilde{z}_i)$  denotes the set of manually defined neighboring symbol indices based on the topology of  $\mathbf{s}_{\tilde{z}_i}$ . This regularization is implemented by

$$\mathcal{L}_{\text{SOM}} = \mathbb{E}_{\mathbf{X}} \left[ \sum_{i=1}^N \sum_{j \in \mathbb{N}(\tilde{z}_i)} \lambda_{ij} \text{MSE}(\mathbf{c}_j, \text{sg}(\mathbf{y}_i)) \right], \quad (13)$$

where  $\lambda_{ij}$  is a weighting coefficient inversely proportional to the Euclidean distance between symbols  $\mathbf{s}_i$  and  $\mathbf{s}_j$ .

Following [19], we define  $\mathbb{N}(\tilde{z}_i)$  as the four nearest neighbors (up, down, left, and right) on the constellation map, and set  $\lambda_{ij} = 1$ . When fewer than four neighbors exist, only the available ones are used. Finally, the total training objective for the JSCC encoder–decoder and the VQ codebook is given by

$$\mathcal{L}_{\text{VQ-SOM}} = \mathcal{L}_{\text{VQ}} + \gamma \mathcal{L}_{\text{SOM}}, \quad (14)$$

where  $\gamma$  is a balancing coefficient between  $\mathcal{L}_{\text{VQ}}$  and  $\mathcal{L}_{\text{SOM}}$ . By jointly updating the codewords using the SOM regularization, the learned codebook forms a smoother and more topology-preserving manifold in the feature space, analogous to the locality-preserving property of Gray-mapping. The entire training process is summarized in **Algorithm 2**, while the first stage employs  $\mathcal{L}_{\text{VQ-SOM}}$  in (14) instead of  $\mathcal{L}_{\text{VQ}}$  in (12).

### C. Decoding Process with SSCDM

After the training stages, the receiver employs the SSCDM, i.e.,  $\text{DM}_\theta$ , to correct symbol errors prior to image reconstruction, where this whole procedure is presented in **Algorithm 3**. Given the channel SNR  $\eta$  and the predefined noise schedule  $\{\sigma_{t_k}^2\}_{k=1}^T$ , the starting time index  $k^*$  of the reverse diffusion process is determined as

$$k^* = \arg \min_{k \in [1:T]} |\eta - P/\bar{\sigma}_{t_k}^2|, \quad (15)$$

where  $\bar{\sigma}_{t_k}^2 = \sum_{k'=1}^k \sigma_{t_{k'}}^2$ . The current channel condition thus determines the starting time point  $t_{k^*}$  of the reverse diffusion process, where higher SNR corresponds to  $t_{k^*}$  closer to 0 and lower SNR is mapped to  $t_{k^*}$  closer to 1.

The received index vector  $\tilde{\mathbf{z}}$  is then regarded as the perturbed sample  $\mathbf{u}_{t_{k^*}}$  in the discrete DM. Starting from  $t_{k^*}$ , the reverse diffusion proceeds iteratively down to  $t_1$ . At each step  $k$ , the reverse kernel  $p_{t_{k-1}|t_k}^\theta(\mathbf{u}_{t_{k-1}}|\mathbf{u}_{t_k}, \mathbf{C})$  is computed by  $\text{DM}_\theta$  as defined in (11), and  $\mathbf{u}_{t_{k-1}}$  is sampled accordingly. Note that, when computing  $p_{t_{k-1}|t_k}$ ,  $\mathbf{u}_{t_k}$  is projected onto the semantic latent space by replacing it with the corresponding codeword from the learned codebook  $\mathbf{C}$ . To ensure stable reconstruction, once the process reaches  $t_1$ , the final clean data  $\mathbf{u}_{t_0}$  is obtained by computing  $p_{t_0|t_1}^\theta(\mathbf{u}_{t_0}|\mathbf{u}_{t_1}, \mathbf{C})$  via  $\text{DM}_\theta$  and performing maximum-likelihood symbol selection for each entry, rather than stochastic sampling. The corrected index vector is thus given by  $\hat{\mathbf{z}} = \mathbf{u}_{t_0}$ . The above operations correspond to lines 2-10 of **Algorithm 3**, i.e.,  $\hat{\mathbf{z}} = \text{DM}_\theta(\tilde{\mathbf{z}}, \eta, \mathbf{C})$  in Section III. Finally,  $\hat{\mathbf{z}}$  is dequantized into the discretized feature representation  $\hat{\mathbf{Y}}$  using the codebook  $\mathbf{C}$ , and the JSCC decoder  $g_{\psi_{\text{Rx}}}$  reconstructs the image  $\hat{\mathbf{X}}$ .

## VI. EXPERIMENTAL RESULTS

In this section, we evaluate the performance of the proposed SSCDM by employing two standard image reconstruction metrics: the multi-scale structural similarity index measure (MS-SSIM) and the learned perceptual image patch similarity (LPIPS), where higher MS-SSIM and lower LPIPS indicate better image quality. Experiments are conducted on the FFHQ dataset [24], which consists of color images with a high resolution of  $256 \times 256$ . The NN architecture follows the residual convolutional neural network (CNN)-based design in [12], adapted for the FFHQ dataset by setting  $c_1 = 128$  and  $c_2 = 256$ , with both the encoder and decoder consisting of five layers. This configuration results in a compression ratio of  $\frac{N}{CHW} = \frac{1}{192}$ .

We assume 16-QAM modulation<sup>5</sup> for transmission, leading to a codebook size of 16, and each codeword is represented as a 4-dimensional vector. The batch size is set to 32, and the learning rate is initialized to 0.01 with a step decay scheduler, where the decay rate is 0.5 and the decay period is 80 epochs. The total number of training epochs is 400, and the training SNR is fixed at  $\eta_{\text{train}} = 20$  dB to ensure sufficiently reliable symbol observations, while the DM is applied under lower SNR regimes. For optimizing the JSCC encoder-decoder and the VQ codebook in the first training stage, the hyperparameters in  $\mathcal{L}_{\text{VQ-SOM}}$  are configured as  $\alpha = 1$ ,  $\beta = 0.25$ , and  $\gamma = 0.9$ .

To optimize SSCDM, a set of Markov-enforced matrices  $\{\mathbf{Q}_{t_k|t_0}\}_{k=1}^T$  with  $t_k = k/T$  must be predetermined, which are obtained through **Algorithm 1** and then the cubic spline interpolation. The hyperparameters in the loss function (10) are  $\lambda_1 = \lambda_2 = 10$ . We set the maximum diffusion step to  $T = 100$ , and the noise variance sequence  $\{\sigma_{t_k}^2\}_{k=1}^T$  is designed using the sigmoid-based scheduling method described in Appendix D, covering the SNR range from  $-3$  dB to 15 dB. For the subsequence  $\{t_{k_\ell}\}_{\ell=1}^{T'}$  with  $T' = 10$ , the time steps are manually chosen to be denser near the beginning and the end of the full sequence  $\{t_k\}_{k=1}^T$ . Specifically, we set

$\{k_\ell\}_{\ell=1}^{T'} = \{2, 4, 9, 20, 40, 65, 84, 94, 98, 100\}$  as indicated by the vertical lines in Fig. 2.

For DM-based digital symbol error correction modules, we adopt U-Net as the backbone architecture, commonly employed for DMs such as DDPM [1] and D3PM [3]. The DM input corresponds to the feature map composed of the VQ codeword indices from the symbol detection. This input is first expanded to a base tensor channel dimension  $\kappa$  through an input layer, followed by three down-sampling and up-sampling stages. During these stages, self-attention is applied at the resolution of  $16 \times 16$ . In the second training stage, the DM is optimized via  $\mathcal{L}_\lambda$  with  $\lambda = 0.001$ . The batch size and learning rate are set to 32 and  $2 \times 10^{-4}$ , respectively, and the total training iteration is 400,000.

For the comparative analysis, we consider the following baselines. The JSCC encoder-decoder and the VQ codebook for all the baselines are trained using  $\mathcal{L}_{\text{VQ-SOM}}$  defined in (14).

- **VQ-JSCC**: This method serves as the baseline model without the DM module. It is trained solely in the first stage of **Algorithm 2**.
- **CD3M [14]**: This method applies D3PM [3] for symbol-level error correction in digital semantic communication. CD3M estimates per-step transition matrices independently by fitting a step-wise transition matrix between consecutive symbol detection matrices. The training configurations largely follow those reported in [14]. For a fair comparison, the scale factor of the noise scheduler is set to 0.9976 to match the target SNR range, with an identical model architecture to ours.
- **DCDDM [15]**: This method also utilizes D3PM [3] for discrete DM to perform digital symbol correction. Each transition matrix includes a diagonal term representing correct transmission, while the remaining probability is allocated to other symbols in proportion to their pairwise symbol error probabilities. The overall model architecture and training settings are aligned with those of SSCDM. For the unspecified noise variance sequence in [15], we adopt a commonly used linear scheduling strategy.
- **SCDM [16]**: This method adopts the score-based DM [2], where continuous diffusion is applied to denoise AWGN-corrupted digital symbols before symbol detection. We follow the training procedure described in [16], while the size of DM in [2] is adjusted to match that of other methods for a fair comparison.

### A. Transition Matrix Similarity

Fig. 3 presents the heatmaps of 16-QAM transition matrices under varying SNR conditions. The proposed SSCDM successfully preserves the Markov property while accurately reflecting the characteristics of digital communication channel, as evidenced by the strong visual similarity between the ground-truth transition matrices (first row) and those by SSCDM (second row). In contrast, DCDDM (third row) exhibits clear discrepancies from the ground truth, mainly due to the absence of a proper Markov-chain formulation and inadequate modeling of channel dynamics.

To quantitatively assess the similarity between transition matrices, we compute the normalized mean square error

<sup>5</sup>Our method is not restricted to a specific modulation order and can be directly extended to other constellations by adjusting the codebook size.

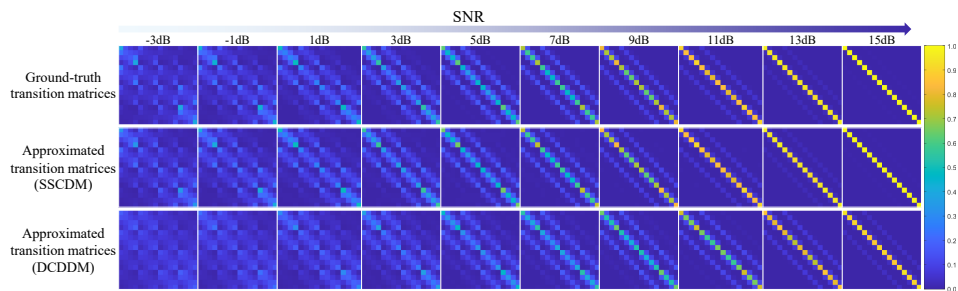


Fig. 3. Heatmaps of 16-QAM transition matrix for the ground-truth, SSCDM, and DCDDM under different SNR conditions.

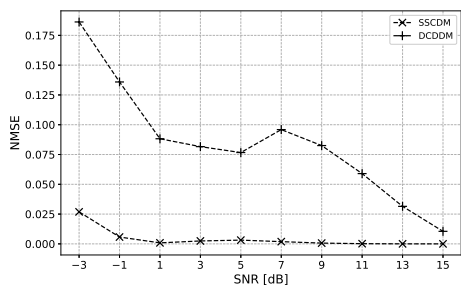


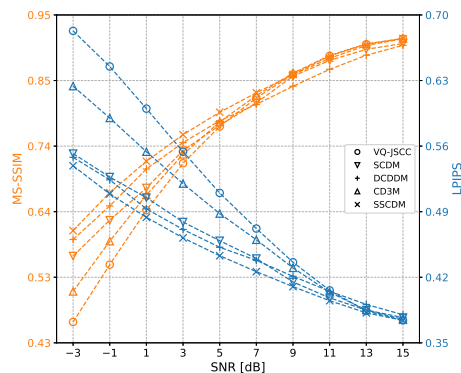
Fig. 4. NMSE of the designed transition matrices of SSCDM and DCDDM.

(NMSE), i.e.,  $\|\mathbf{Q}_{t_k|t_0} - \hat{\mathbf{Q}}_{t_k|t_0}\|_F^2 / \|\mathbf{Q}_{t_k|t_0}\|_F^2$ , where  $\mathbf{Q}_{t_k|t_0}$  denotes the ground-truth transition matrix and  $\hat{\mathbf{Q}}_{t_k|t_0}$  represents the obtained one from SSCDM. In Fig. 4, the NMSE of SSCDM converges to nearly zero across all SNR regions, confirming its ability to precisely capture the true channel transition behavior. In contrast, the approximated matrices from DCDDM exhibit noticeable errors relative to the ground truth. These results collectively validate the effectiveness of the proposed optimization method in **Algorithm 1**. Consequently, SSCDM successfully models the underlying channel dynamics while preserving the Markov property, thereby enabling more stable and reliable diffusion-based correction.

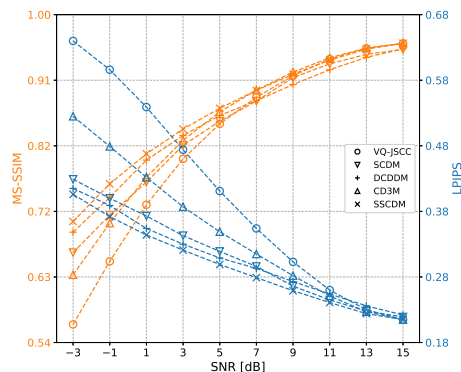
### B. Comparison with Baselines

As shown in Fig. 5(a), our method consistently surpasses all baselines across the full SNR range, with particularly pronounced gains in low-SNR regions. While other DM-based schemes also enhance performance compared to VQ-JSCC, SSCDM delivers a more significant advantage by constructing transition matrices that both reflect the characteristics of digital communication channels and preserve the Markov property required by the DM. As the SER drops sharply in high-SNR regions, both SCDM and DCDDM are slightly inferior to VQ-JSCC. This indicates that the continuous DM employed in SCDM is less suitable for AWGN denoising in digital communication, whereas the heuristic transition matrices of DCDDM fail to represent discrete diffusion precisely for symbol correction. In contrast, SSCDM maintains comparable performance to VQ-JSCC even at high SNRs, owing to our principled design of transition matrices. While CD3M attains competitive performance in high-SNR conditions, its gains in low-SNR regimes remain limited compared to other methods, primarily because it directly employs symbol detection matrices that are intrinsically non-Markovian.

Furthermore, as illustrated in Fig. 6, SSCDM delivers more stable and coherent reconstructions, whereas other schemes often exhibit degraded image quality with noticeable artifacts



(a) FFHQ



(b) CelebA

Fig. 5. MS-SSIM $\uparrow$  (orange) and LPIPS $\downarrow$  (blue) comparison between SSCDM and baseline methods on (a) FFHQ and (b) CelebA datasets.

or structural distortions. Consequently, our method yields smoother and more perceptually faithful reconstructions in both quantitative and qualitative evaluations. To further validate the robustness of our approach, we conduct additional experiments on the CelebA dataset [25], consisting of  $128 \times 128$  color images. The model configuration is adapted from the FFHQ experiments by setting  $c_1 = 64$  and  $c_2 = 128$ , with both the encoder and decoder composed of four layers, resulting in a compression ratio of  $\frac{N}{CHW} = \frac{1}{48}$ . As depicted in Fig. 5(b), SSCDM exhibits performance trends similar to those observed on FFHQ, consistently outperforming other methods across all SNR levels. These results demonstrate that our method maintains stable performance for other datasets.

### C. Impact of Codebook-Guided U-Net Embedding

As described in Section IV-C, we incorporate the codebook embedding into the U-Net input to strengthen the integration of the DM within the overall JSCC framework. By aligning

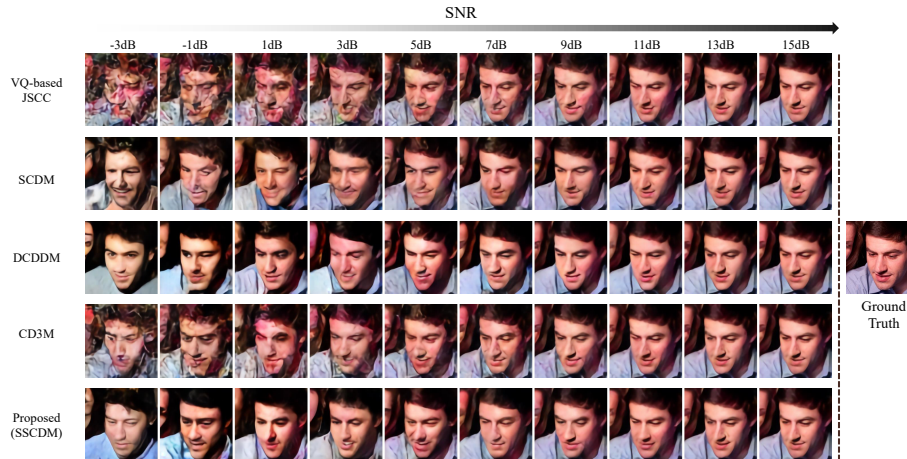


Fig. 6. Reconstructed images from SSCDM and baseline methods with varying SNRs.

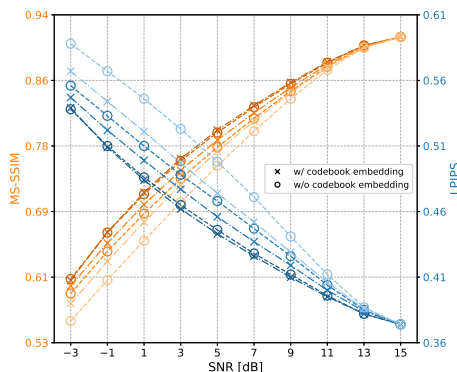


Fig. 7. MS-SSIM $\uparrow$  (orange) and LPIPS $\downarrow$  (blue) comparison between SSCDM with and without codebook embedding across different base tensor channel dimensions  $\kappa$  of the U-Net. Darker colors are larger  $\kappa$  (16  $\rightarrow$  32  $\rightarrow$  64).

the diffusion process with the latent semantic space of the JSCC decoder, this design enables the DM to more effectively capture semantic relationships among codewords. Fig. 7 clearly shows that the embedding-based approach consistently outperforms the one without embedding. The performance gap becomes more pronounced as  $\kappa$  decreases, i.e., the model size is reduced, indicating a limitation in representational capacity. By injecting codebook-level semantic structure, the proposed embedding enables the DM to exploit richer semantic information and mitigates performance degradation in compact models. As a result, the DM achieves more stable and semantically coherent symbol correction with only a negligible parameter overhead of 1.8K.

#### D. Effect of SOM-Based Codebook Learning

Fig. 8 illustrates the Euclidean distances between the learned codewords and four randomly selected reference codewords, i.e.,  $c_1$ ,  $c_7$ ,  $c_{12}$ , and  $c_{14}$ . When trained solely with  $\mathcal{L}_{VQ}$ , no mechanism enforces local consistency in the feature space. Consequently, the distance pattern does not exhibit a smoothly increasing transition from the reference codewords. The codebook reordering (CR) algorithm [17] reorders codewords by greedily finding the minimum distance codeword and then applies Gray coding after the codebook optimization with  $\mathcal{L}_{VQ}$ . Although the CR approach attempts to enhance the locality, it still fails to preserve meaningful spatial relationships between codewords. This is mainly because this method is heuristic



Fig. 8. Heatmaps of Euclidean distances between each codeword constructed by using  $\mathcal{L}_{VQ}$ ,  $\mathcal{L}_{VQ} + CR$ , and  $\mathcal{L}_{VQ-SOM}$ .

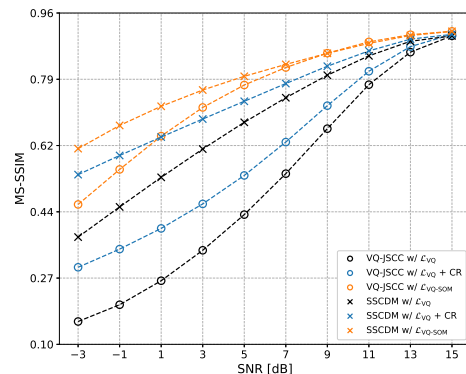


Fig. 9. MS-SSIM $\uparrow$  comparison between VQ codebook construction methods without and with symbol error correction by SSCDM.

and lacks a learning-based adaptation. In contrast, our SOM-based method trained with  $\mathcal{L}_{VQ-SOM}$  successfully establishes a smooth and topology-preserving structure in the codebook. The heatmaps clearly demonstrate this property through gradual color transitions, indicating progressively increasing distances from the reference codewords.

The Euclidean distance property illustrated in Fig. 8 directly

translates into the image reconstruction performance shown in Fig. 9. Specifically, the SOM-aided SSCDM achieves remarkably better performance than SSCDM with  $\mathcal{L}_{VQ}$  or combined with the CR algorithm. In the two baseline variants using SSCDM with  $\mathcal{L}_{VQ}$ , the VQ codebook fails to maintain local consistency in the constellation space, preventing SSCDM from effectively linking its error correction capability to downstream task performance. In contrast, our SOM-based learning produces a topology-preserving codebook, enabling SSCDM's error correction process to more effectively enhance image reconstruction performance compared to VQ-JSCC with  $\mathcal{L}_{VQ-SOM}$ . Moreover, performance improvements are consistently observed across all codebook construction methods when integrated with SSCDM, confirming the effective error-correcting capability of the proposed SSCDM.

## VII. CONCLUSION

This work introduced SSCDM, a novel semantic symbol correcting DM tailored for VQ-based digital semantic communication under a discrete-time diffusion framework. By enforcing Markov-consistent transition dynamics for discrete symbols using a CTMC solution and embedding them into a semantic latent space, our approach transforms the inherently non-Markovian symbol transitions induced by realistic digital communication channels into a tractable form, enabling principled and robust symbol correction. Moreover, a SOM-based regularization is incorporated into the codebook learning to preserve the geometric vicinity of neighboring symbols, further enhancing correction reliability and reconstruction fidelity. Comprehensive experiments under various channel conditions and datasets confirm that SSCDM outperforms existing baselines, particularly in low-SNR regimes.

### APPENDIX A PROOF OF THEOREM 1

We prove the theorem by comparing the two expressions  $[\mathbf{Q}_{t_k|t_0}]_{i,j}$  and  $[\mathbf{Q}_{t_{k-1}|t_0} \mathbf{Q}_{t_k|t_{k-1}}]_{i,j}$ , both of which describe the transition probability from a single symbol point  $\mathbf{s}_i$  at time point  $t_0$  to region  $\mathbb{A}_j$  at time point  $t_k$ .

By the definition of cumulative variance  $\bar{\sigma}_{t_k}^2 = \bar{\sigma}_{t_{k-1}}^2 + \sigma_{t_k}^2$ , the direct transition  $\mathbf{Q}_{t_k|t_0}$  is given by

$$\begin{aligned} [\mathbf{Q}_{t_k|t_0}]_{i,j} &= \iint_{\mathbb{A}_j} \frac{1}{2\pi\bar{\sigma}_{t_k}^2} e^{-\frac{\|\mathbf{x}-\mathbf{s}_i\|_2^2}{\bar{\sigma}_{t_k}^2}} d\mathbf{x} \\ &= \sum_{u=1}^M \iint_{\mathbb{A}_u} \frac{1}{2\pi\bar{\sigma}_{t_{k-1}}^2} e^{-\frac{\|\mathbf{x}'-\mathbf{s}_i\|_2^2}{\bar{\sigma}_{t_{k-1}}^2}} \\ &\quad \times \iint_{\mathbb{A}_j} \frac{1}{2\pi\sigma_{t_k}^2} e^{-\frac{\|\mathbf{x}-\mathbf{x}'\|_2^2}{\sigma_{t_k}^2}} d\mathbf{x}d\mathbf{x}'. \end{aligned} \quad (16)$$

The second equality reflects a sequential corruption process, where two independent Gaussian noises  $n_1 \sim \mathcal{CN}(0, \bar{\sigma}_{t_{k-1}}^2)$  and  $n_2 \sim \mathcal{CN}(0, \sigma_{t_k}^2)$  are successively applied to the symbol  $\mathbf{s}_i$ . Each term in the summation over  $u \in [1:M]$  represents a path where the first noise perturbs  $\mathbf{s}_i$  to a specific point  $\mathbf{x}' \in \mathbb{A}_u$ , and the second noise moves this exactly same point  $\mathbf{x}'$  into the region  $\mathbb{A}_j$ . In other words, the product of probabilities is taken for the same intermediate point  $\mathbf{x}'$  before integration.

On the other hand, the matrix product yields

$$\begin{aligned} [\mathbf{Q}_{t_{k-1}|t_0} \mathbf{Q}_{t_k|t_{k-1}}]_{i,j} &= \sum_{u=1}^M \iint_{\mathbb{A}_u} \frac{1}{2\pi\bar{\sigma}_{t_{k-1}}^2} e^{-\frac{\|\mathbf{x}-\mathbf{s}_i\|_2^2}{\bar{\sigma}_{t_{k-1}}^2}} d\mathbf{x} \\ &\quad \times \iint_{\mathbb{A}_u} \frac{a_{t_{k-1}}(\mathbf{x}')}{b_{t_{k-1}}(u)} \iint_{\mathbb{A}_j} \frac{1}{2\pi\sigma_{t_k}^2} e^{-\frac{\|\mathbf{x}'-\mathbf{x}''\|_2^2}{\sigma_{t_k}^2}} d\mathbf{x}'d\mathbf{x}'' \end{aligned} \quad (17)$$

In this case, the integral over the intermediate region  $\mathbb{A}_u$  effectively includes contributions from products of probabilities corresponding to different points  $\mathbf{x}$  and  $\mathbf{x}''$  within the same region. That is, transitions from  $\mathbf{s}_i$  at  $t_0$  to  $\mathbf{x} \in \mathbb{A}_u$  at  $t_{k-1}$  combined with  $\mathbf{x}' \in \mathbb{A}_u$  at  $t_{k-1}$  to  $\mathbf{x}'' \in \mathbb{A}_j$  at  $t_k$  for  $\mathbf{x} \neq \mathbf{x}''$  also enter the calculation.

Consequently, the two expressions are mathematically and fundamentally distinct, since the difference in their underlying  $\sigma$ -algebras directly causes them to integrate over *different sets of events*. The true probability in (16) is conditioned on the fine-grained, point-refined  $\sigma$ -algebra  $\mathcal{F}_{t_{k-1}} = \sigma(X_{t_{k-1}})$ . Conditioning on  $\mathcal{F}$  necessitates computing *an integral of a product*, thereby correctly accounting only for paths that pass through the *same intermediate point*  $\mathbf{x}'$ , conceptually expressed as

$$\begin{aligned} (\mathbf{s}_i \rightarrow \mathbb{A}_u \rightarrow \mathbb{A}_j) &= \sum_{\mathbf{x}' \in \mathbb{A}_u} (\mathbf{s}_i \rightarrow \mathbf{x}' \rightarrow \mathbb{A}_j) \\ &= \sum_{\mathbf{x}' \in \mathbb{A}_u} (\mathbf{s}_i \rightarrow \mathbf{x}') \times (\mathbf{x}' \rightarrow \mathbb{A}_j). \end{aligned} \quad (18)$$

In contrast, the Chapman-Kolmogorov composition in (17) forces conditioning on the coarse, region-based  $\sigma$ -algebra  $\mathcal{G}_{t_{k-1}} = \sigma(\{X_{t_{k-1}} \in \mathbb{A}_u\})$ . This conditioning on  $\mathcal{G}$ , i.e., a strictly coarser sub- $\sigma$ -algebra of  $\mathcal{F}$ , compels the calculation into the form of a *product of integrals*. This structure inherently includes paths that originate and depart from *different intermediate points*  $\mathbf{x} \neq \mathbf{x}''$  at  $t_{k-1}$ , informally written as

$$\begin{aligned} (\mathbf{s}_i \rightarrow \mathbb{A}_u \rightarrow \mathbb{A}_j) &= \sum_{\mathbf{x} \in \mathbb{A}_u} (\mathbf{s}_i \rightarrow \mathbf{x}) \times \sum_{\mathbf{x}'' \in \mathbb{A}_u} (\mathbf{x}'' \rightarrow \mathbb{A}_j) \\ &= \sum_{\mathbf{x}, \mathbf{x}'' \in \mathbb{A}_u} (\mathbf{s}_i \rightarrow \mathbf{x}) \times (\mathbf{x}'' \rightarrow \mathbb{A}_j). \end{aligned} \quad (19)$$

Since these two probability measures are defined over *non-identical event spaces*, we conclude that  $[\mathbf{Q}_{t_k|t_0}]_{i,j} \neq [\mathbf{Q}_{t_{k-1}|t_0} \mathbf{Q}_{t_k|t_{k-1}}]_{i,j}$ , thereby violating the Chapman-Kolmogorov equation and formally establishing the non-Markovian nature of the process.

### APPENDIX B PROOF OF LEMMA 1

To investigate the sign of the eigenvalues of the rate matrix, we introduce a matrix  $\mathbf{P} = \overrightarrow{\mathbf{R}}_t + \mathbf{I}_M \in \mathbb{R}^{M \times M}$ , where adding the identity matrix converts the rate matrix into a row-stochastic matrix. Since the rate matrix  $\overrightarrow{\mathbf{R}}_t \in \mathbb{R}^{M \times M}$  has non-positive diagonal entries and non-negative off-diagonal entries according to **Proposition 1**, all entries of  $\mathbf{P}$  are non-negative. As  $\overrightarrow{\mathbf{R}}_t$  has the zero row-sum property from **Proposition 1**, i.e.,  $\sum_{j=1}^M [\overrightarrow{\mathbf{R}}_t]_{i,j} = 0$  for  $i \in [1:M]$ ,  $\mathbf{P}$  is row-stochastic with satisfying  $\sum_{j=1}^M [\mathbf{P}]_{i,j} = 1$  for  $i \in [1:M]$ . Moreover, since the rate matrix can be eigen-decomposed into  $\overrightarrow{\mathbf{R}}_t = \mathbf{V}\Sigma(t)\mathbf{V}^{-1}$  as in (6), we can express  $\mathbf{P}$  as

$\mathbf{P} = \overrightarrow{\mathbf{R}}_t + \mathbf{I}_M = \mathbf{V}(\boldsymbol{\Sigma}(t) + \mathbf{I}_M)\mathbf{V}^{-1} = \mathbf{V}\boldsymbol{\Lambda}\mathbf{V}^{-1}$ , where  $\boldsymbol{\Lambda} = \boldsymbol{\Sigma}(t) + \mathbf{I}_M \in \mathbb{R}^{M \times M}$ .

**Lemma 2.** *The largest eigenvalue of any row-stochastic matrix is 1.*

*Proof:* See Appendix C.  $\blacksquare$

Since  $\mathbf{P}$  is row-stochastic, **Lemma 2** implies that  $[\boldsymbol{\Lambda}]_{i,i} \leq 1$  for  $i \in [1:M]$ . Therefore, because  $\boldsymbol{\Lambda} = \boldsymbol{\Sigma}(t) + \mathbf{I}_M$ , each diagonal element of  $\boldsymbol{\Sigma}(t)$  is non-positive. Recall that  $\mathbf{D}(t) = \exp(\int_0^t \boldsymbol{\Sigma}(t')dt')$ , where  $\mathbf{D}(t)$  comes from the eigen-decomposition of  $\mathbf{Q}_{t|0} = \mathbf{V}\mathbf{D}(t)\mathbf{V}^{-1}$  as in (5). As a result, the integral  $\int_0^t \boldsymbol{\Sigma}(t')dt'$  is non-increasing in  $t$ , and thus each diagonal element  $[\mathbf{D}(t)]_{i,i}$  is also non-increasing in  $t$ . Hence, the sequence  $\{[\mathbf{D}(t_k)]_{i,i}\}_{k=0}^T$  is non-increasing for  $i \in [1:M]$ .

## APPENDIX C

### PROOF OF LEMMA 2

Let  $\mathbf{P} \in \mathbb{R}^{M \times M}$  be a row-stochastic matrix, i.e.,  $[\mathbf{P}]_{j,:} \mathbf{1}_M = 1$  for  $j \in [1:M]$ , and suppose it admits the eigen-decomposition  $\mathbf{V}\boldsymbol{\Lambda}\mathbf{V}^{-1}$ . For contradiction, suppose that there exists an eigenvalue  $[\boldsymbol{\Lambda}]_{i,i} > 1$  for some  $i \in [1:M]$ , where  $[\mathbf{V}]_{:,i}$  is the corresponding eigenvector. Without loss of generality, let  $j$  be an index such that  $[\mathbf{V}]_{j,i} = \max_{k \in [1:M]} [\mathbf{V}]_{k,i} > 0$ . Then, by the eigenvalue relation, we have  $[\mathbf{P}]_{j,:} [\mathbf{V}]_{:,i} = [\mathbf{V}]_{j,i} [\boldsymbol{\Lambda}]_{i,i} > [\mathbf{V}]_{j,i}$ , which contradicts  $[\mathbf{P}]_{j,:} [\mathbf{V}]_{:,i} \leq [\mathbf{P}]_{j,:} ([\mathbf{V}]_{j,i} \mathbf{1}_M) = [\mathbf{V}]_{j,i} ([\mathbf{P}]_{j,:} \mathbf{1}_M) = [\mathbf{V}]_{j,i}$ . Therefore, no eigenvalue of  $\mathbf{P}$  can exceed 1, and since  $\mathbf{P} \mathbf{1}_M = 1 \cdot \mathbf{1}_M$ , the largest eigenvalue is exactly 1.

## APPENDIX D

### NOISE SCHEDULING METHOD

Our noise scheduling follows the sigmoid-based formula presented in Algorithm 4 of [20]. The standard form of the scheduling function for  $0 \leq t \leq 1$  is expressed as

$$\omega_t = \frac{\text{sig}(t(\nu_{\text{end}} - \nu_{\text{start}}) + \nu_{\text{start}}) - \text{sig}(\nu_{\text{start}})}{\text{sig}(\nu_{\text{end}}) - \text{sig}(\nu_{\text{start}})}, \quad (20)$$

where  $\text{sig}(x) = 1/(1 + e^{-x})$  denotes the sigmoid function, and  $\nu_{\text{start}}$  and  $\nu_{\text{end}}$  control the curvature of the scheduling curve. We employ this formulation to design a noise scheduling function that outputs the SNR  $\bar{\eta}_{t_k}$  in dB scale at time points  $t_k$  with  $k \in [1:T]$ , where  $t_0 = 0$  and  $0 < t_k \leq 1$ . Accordingly, for  $k \in [1:T]$ ,  $\bar{\eta}_{t_k}$  in dB scale is defined as

$$\bar{\eta}_{t_k} [\text{dB}] = \xi_1 \times 10 \cdot \log_{10} \left( \frac{1 - \omega_{t_{k-1}}}{\omega_{t_{k-1}}} \right) + \xi_2, \quad (21)$$

where  $\xi_1$  and  $\xi_2$  are scaling and offset parameters, respectively. The relationship between  $\bar{\eta}_{t_k} [\text{dB}]$  and the noise variance sequence  $\{\sigma_{t_k}\}_{k=1}^T$  is given by  $\bar{\eta}_{t_k} [\text{dB}] = 10 \cdot \log_{10}(P/\bar{\sigma}_{t_k}^2)$ , where  $\bar{\sigma}_{t_k}^2 = \sum_{k'=1}^k \sigma_{t_{k'}}^2$ . In our experiments, we set  $\nu_{\text{start}} = 0.025$ ,  $\nu_{\text{end}} = 1.25$ ,  $\xi_1 = 0.45$  and  $\xi_2 = 6.5$ .

## REFERENCES

[1] J. Ho, A. Jain, and P. Abbeel, “Denosing diffusion probabilistic models,” *Advances in Neural Information Processing Systems (NeurIPS)*, vol. 33, pp. 6840–6851, 2020.

[2] Y. Song, J. Sohl-Dickstein, D. P. Kingma, A. Kumar, S. Ermon, and B. Poole, “Score-based generative modeling through stochastic differential equations,” *arXiv preprint arXiv:2011.13456*, 2020.

[3] J. Austin, D. D. Johnson, J. Ho, D. Tarlow, and R. Van Den Berg, “Structured denoising diffusion models in discrete state-spaces,” *Advances in Neural Information Processing Systems (NeurIPS)*, vol. 34, pp. 17981–17993, 2021.

[4] A. Campbell, J. Benton, V. De Bortoli, T. Rainforth, G. Deligiannidis, and A. Doucet, “A continuous time framework for discrete denoising models,” *Advances in Neural Information Processing Systems (NeurIPS)*, vol. 35, pp. 28266–28279, 2022.

[5] H. Sun, L. Yu, B. Dai, D. Schuurmans, and H. Dai, “Score-based continuous-time discrete diffusion models,” *arXiv preprint arXiv:2211.16750*, 2022.

[6] L. Yang, Z. Zhang, Y. Song, S. Hong, R. Xu, Y. Zhao, W. Zhang, B. Cui, and M.-H. Yang, “Diffusion models: A comprehensive survey of methods and applications,” *ACM computing surveys*, vol. 56, no. 4, pp. 1–39, 2023.

[7] Y. Shi, Y. Zhou, D. Wen, Y. Wu, C. Jiang, and K. B. Letaief, “Task-oriented communications for 6G: Vision, principles, and technologies,” *IEEE Wireless Communications*, vol. 30, no. 3, pp. 78–85, 2023.

[8] X. Luo, H.-H. Chen, and Q. Guo, “Semantic communications: Overview, open issues, and future research directions,” *IEEE Wireless Communications*, vol. 29, no. 1, pp. 210–219, 2022.

[9] D. Gündüz, M. A. Wigger, T.-Y. Tung, P. Zhang, and Y. Xiao, “Joint source–channel coding: Fundamentals and recent progress in practical designs,” *Proceedings of the IEEE*, pp. 1–32, 2024.

[10] Y. Huh, B. Kim, and W. Choi, “Feature reconstruction aided federated learning for image semantic communication,” in *IEEE Global Communications Conference (GLOBECOM)*, 2025, pp. 1–6.

[11] —, “Federated learning enhanced by feature reconstruction for semantic communication module updates of agents,” *arXiv preprint arXiv:2508.03248*, 2025.

[12] Y. Huh, H. Seo, and W. Choi, “Universal joint source-channel coding for modulation-agnostic semantic communication,” *IEEE Journal on Selected Areas in Communications*, vol. 43, no. 7, pp. 2560–2574, 2025.

[13] E. Kim, Y. Huh, and W. Choi, “Extended universal joint source-channel coding for digital semantic communications: Improving channel-adaptability,” *arXiv preprint arXiv:2602.14018*, 2026.

[14] W. Tang, Z. Meng, Q. Li, M. Yan, and X. Ge, “Channel denoising in digital semantic communication systems via discrete diffusion,” *IEEE Wireless Communications Letters*, vol. 15, pp. 1035–1039, 2026.

[15] G. He, S. Zhang, and T. Jiang, “Residual vector quantized diffusion model-based joint source-channel coding for task-oriented agent communication,” *IEEE Transactions on Wireless Communications*, vol. 24, no. 6, pp. 4663–4676, 2025.

[16] H. Mo, Y. Sun, S. Yao, H. Chen, Z. Chen, X. Xu, N. Ma, M. Tao, and S. Cui, “SCDM: Score-based channel denoising model for digital semantic communications,” in *IEEE International Conference on Communications (ICC)*, 2025, pp. 3772–3778.

[17] Y. Zhou, Y. Sun, G. Chen, X. Xu, H. Chen, B. Huang, S. Cui, and P. Zhang, “MOC-RVQ: Multilevel codebook-assisted digital generative semantic communication,” in *IEEE Global Communications Conference (GLOBECOM)*, 2024, pp. 2078–2083.

[18] T. Kohonen, “The self-organizing map,” *Proceedings of the IEEE*, vol. 78, no. 9, pp. 1464–1480, 2002.

[19] V. Fortuin, M. Hüser, F. Locatello, H. Strathmann, and G. Rätsch, “SOM-VAE: Interpretable discrete representation learning on time series,” *arXiv preprint arXiv:1806.02199*, 2018.

[20] A. Jabri, D. Fleet, and T. Chen, “Scalable adaptive computation for iterative generation,” *arXiv preprint arXiv:2212.11972*, 2022.

[21] S. McKinley and M. Levine, “Cubic spline interpolation,” *College of the Redwoods*, vol. 45, no. 1, pp. 1049–1060, 1998.

[22] O. Ronneberger, P. Fischer, and T. Brox, “U-Net: Convolutional networks for biomedical image segmentation,” in *International Conference on Medical Image Computing and Computer-Assisted Intervention (MICCAI)*, 2015, pp. 234–241.

[23] A. Van Den Oord, O. Vinyals *et al.*, “Neural discrete representation learning,” *Advances in Neural Information Processing Systems (NeurIPS)*, vol. 30, 2017.

[24] T. Karras, S. Laine, and T. Aila, “A style-based generator architecture for generative adversarial networks,” in *IEEE/CVF Conference on Computer Vision and Pattern Recognition (CVPR)*, 2019, pp. 4401–4410.

[25] Z. Liu, P. Luo, X. Wang, and X. Tang, “Deep learning face attributes in the wild,” in *IEEE International Conference on Computer Vision (ICCV)*, 2015, pp. 3730–3738.